



HELSINKI UNIVERSITY OF TECHNOLOGY
Department of Electrical and Communications Engineering
Laboratory of Computational Engineering

Klaus Kyttä

Computational Studies of Pattern Formation in Multiple Layer Turing Systems

In partial fulfillment of the requirements for the degree of Master of Science

Supervisor: Professor Kimmo Kaski

Instructor: Professor Rafael Barrio

Espoo 5th January 2007



TEKNILLINEN KORKEAKOULU
HELSINKI UNIVERSITY OF TECHNOLOGY

Helsinki University of Technology
Laboratory of Computational Engineering
Innopoli 2, Tekniikantie 14
P.O.Box 9203
FI-02015 TKK
FINLAND
Tel. +358 9 451 4826
Fax. +358 9 451 4833
<http://www.lce.hut.fi>

E-mail: klaus.kytta@tkk.fi

Tekijä: Klaus Kyttä
Otsikko: Laskennallisia tutkimuksia kuvionmuodostuksesta monikerroksisissa Turing-systeemeissä

Päivämäärä: 5.1.2007 **Sivumäärä:** 87

Osasto: Sähkö- ja tietoliikennetekniikan osasto
Professuuri: S-114, Laskennallinen tekniikka

Valvoja: Professori Kimmo Kaski
Ohjaaja: Professori Rafael Barrio

Tämä diplomityö käsittelee brittiläisen matemaatikon Alan Turingin ehdottamia Turingin systeemeiksi kutsuttuja reaktio-diffuusio systeemejä. Kahden viime vuosikymmenen aikana on julkaistu paljon Turingin kuvioita käsitteleviä tutkimuksia. Osittain tämä johtuu siitä, että nykyiset tietokoneet mahdollistavat näiden numeerisen käsittelyn, mutta toisaalta myös viimeaikaiset löydöt ovat osaltaan vauhdittaneet tutkimusta.

Tässä diplomityössä käsitellään Turing systeemejä ja esitetään tuloksia kerroksellisista systeemeistä. Kuvionmuodostuksen kannalta Turingin systeemejä on tutkittu jo pitkään, mutta vasta viime aikoina on ryhdytty tutkimaan useamman systeemin välistä vuorovaikutusta. Useinmiten kytkentä on suoritettu lineaarisesti, mutta tässä työssä tutkitaan epälineaarisen kytkennän tuomia mahdollisuuksia, mitä ei ole aiemmin numeerisesti tutkittu huolimatta sen tarjoamista mielenkiintoisista sovelluskohteista.

Motivaatiomme näiden systemien tutkimiselle on sekä biologinen että tekninen. Sovelluskohteista voidaan mainita sydänsolujen kalsiumaallot ja impulssien eteneminen hermosoluissa. Toistaiseksi todellisten mallien luominen on osoittautunut liian haasteelliseksi, mutta joitain yksinkertaisia tilanteita on jo pystytty simuloimaan.

Avainsanat: Turingin systeemi, reaktio-diffuusioyhtälö, kuvionmuodostus

Author:	Klaus Kyttä	
Title:	Computational Studies of pattern formation in multiple layer Turing systems	
Date:	5.1.2007	Number of pages: 87
Department:	Electrical and Communications Engineering	
Professorship:	S-114, Computational Engineering	
Supervisor:	Professor Kimmo Kaski	
Instructor:	Professor Rafael Barrio	
<p>This thesis concerns mainly on reaction-diffusion systems, of the kind proposed by a British mathematician Alan Turing in 1950's. During the past two decades a lot of papers have been published dealing with Turing patterns. Partly that is because today's computers make possible to solve those equations accurately in reasonable time but on the other hand the recent findings have also speeded up the research work.</p> <p>In this thesis we present Turing systems in general and show results of coupled systems. From the pattern formation point of view people have studied Turing systems for a long time but only recently there has been growing interest in the interaction of many systems. Usually the coupling has been linear, but we extend the study to non-linear coupling and find out what that brings into the scene. To our knowledge this has not been studied earlier in spite of the intriguing applications it may offer.</p> <p>Our motivation for studying these systems is both biological and technical. For possible applications one can mention calcium waves of cardiac cells and electric impulses in neurons. So far very few real Turing base models have been introduced due to their complexity but a few simple situations can be modeled already.</p>		
Keywords:	Turing system, reaction-diffusion, pattern formation	

Foreword

The research presented in this thesis has been carried out in the Laboratory of Computational Engineering (LCE), Helsinki University of Technology (HUT), during the years 2005-2006, while working as a member of the pattern formation in biological systems research group. The work was started in the summer 2005 when I started my work at LCE as a research student.

First of all I like to thank my supervisor Prof. Kimmo Kaski for introducing me this subject and for giving me the opportunity to combine the research work and my studies. In addition I like to thank him and other personnel, especially my colleagues in room D319, for providing excellent working conditions.

Especially I wish to express my gratitude to Prof. Rafael Barrio (UNAM, México) for his support, guidance and constructive criticism for this thesis. I am also grateful to Prof. Barrio for his hospitality during my two-week visit to the Instituto de Física of Universidad Nacional Autónoma de México.

I thank all my friends outside the LCE for their support and optimism and for being a counterbalance for work and studies.

Lastly, I wish to express my gratitude to my parents for unconditional support.

Otaniemi, 5th January 2007

Klaus Kyttä

Table of Contents

1	Introduction	1
2	Reaction-Diffusion models	4
2.1	Theory of pattern formation	4
2.2	Brusselator model	7
2.2.1	Linear analysis	8
2.2.2	Simulation results	14
2.3	Gray-Scott model	15
2.4	Oregonator model	16
2.5	Lengyel-Epstein model	19
2.6	Barrio-Varea-Aragon-Maini (BVAM) model	20
2.7	Summary	21
3	Numerical methods	23
3.1	Discrete time and solutions of differential equations	23
3.1.1	Euler Method	25
3.1.2	Runge-Kutta Method	25
3.2	Fourier transform and structure factor	27
3.2.1	Discrete Fourier Transform	28
3.2.2	Structure factor	29

3.2.3	Amplitude spectra	30
3.3	Summary	30
4	Analytical methods	32
4.1	Dynamics and stability	32
4.2	Bifurcations	34
4.3	Complex Ginzburg-Landau equation	36
4.4	Amplitude equations	37
4.4.1	Introduction to perturbation theory	38
4.4.2	Square Turing patterns	38
4.4.3	Hexagonal Turing patterns	39
4.4.4	Amplitude equations for BVAM-model	40
4.5	Summary	43
5	Coupled Turing Systems	44
5.1	Two-layer Brusselator model	45
5.1.1	Model	46
5.1.2	Simulation results	48
5.2	Extended Oregonator model	52
5.2.1	Model	52
5.2.2	Simulation results	54
5.3	Cubic coupling	54
5.3.1	Model	55
5.3.2	Simulation results	57
5.3.3	Discussion	61
5.4	Other coupling schemes	64
5.4.1	Quadratic coupling	64

5.4.2	Two-layer BVAM-model	65
6	Conclusions	68
A	Appendix	71
A.1	Forced complex Ginzburg-Landau equation	71

Abbreviations and notations

$\mathbf{U}(\mathbf{r}, t)$	local concentration vector
t	time
Ω	subdomain of space
f_u, f_v, g_u, g_v	partial derivatives
d, D_x	diffusion coefficient for chemical x
$\mathbf{w}_0 = (u_0, v_0)$	steady state of a system
k_i	reaction rate constant
$f(u, v), g(u, v)$	reaction kinetics
\mathbf{k}, k	wave vector, wave number
$\Im(x)$	imaginary part of x
$\Re(x)$	real part of x
λ	wavelength, eigenvalue
$S(k, t)$	structure factor
h	lattice constant, step size
u, v	concentrations of chemicals
\bar{u}	average of u
$C^1(\Omega)$	space of continuously differentiable functions in domain Ω

Chapter 1

Introduction

In 1952 Alan Turing [1] proposed that a system of chemical substances, or morphogens (a word coined by Turing), capable of diffusing and reacting with each other, can produce spatially stable patterns. His aim was to explain pattern formation in real chemical and biological systems and especially to develop a theory for morphogenesis, that is, the ways in which a highly symmetrical egg of an embryo evolves to acquire an anatomical shape. For this he introduced a system of reaction-diffusion equations and determined general conditions for the formation of spatial patterns driven by diffusion. Due to their complexity, more simplified models have been studied but most of the models are built to mimic real systems.

One of the central issues in developmental biology is the formation of spatial patterns in the embryo. In Turing's seminal 1952 article [1] he proposed a model of the growing embryo. Ever since mathematical biologists have been trying to explain some of the essential characteristics of the natural mechanisms of growth. The background of this research was the observation that, for instance, an adult human being consists of tens of trillions of cells (10^{13}) but there are only three billion (3×10^9) base pairs in DNA. So all the information to conform the body cannot be prescribed in detail by the genes, which should only give certain broad guidelines. Therefore, one needs a physical mechanism to convert these guidelines into details. In his paper, Turing showed that a simple mathematical model could solve this problem. The idea was that a chemical pre-pattern is first set up due to a system of reacting and diffusing chemicals, and cells respond to this pre-pattern by differentiating accordingly.

The first observations of chemical oscillating patterns were made a year before Turing's paper by Boris P. Belousov, director of the Institute of Biophysics in the Soviet Union. His paper was rotundly rejected with a critical note from the editor that it was clearly impossible, on the grounds that such

oscillations were thought to be contrary to the Second Law of Thermodynamics. In the 1960's another Russian biophysicist, Anatol M. Zhabotinsky, confirmed Belousov's findings, and it was noticed that the reaction first observed by Belousov exhibits a pattern formation mechanism with similarities to the mechanism Turing had proposed. It was in the 1970's when Gierer and Meinhardt [2] gave a biologically justified formulation of the Turing model, and studied its properties by computer simulations. Since then, the study of biological pattern formation has gained popularity. It was not until 1990 that real Turing patterns were observed in chemical experiments [3].

Turing systems have been shown to be able to, at least qualitatively, mimic many biological patterns such as the stripes of a zebra or colourful patterns on fishes. In Ref. [4] one can find a detailed study of the rôle of patterns in biology and in addition Ref. [5] provides an introduction to the subject. Although reaction-diffusion systems can imitate various biological patterns and a real Turing instability has been reproduced in the laboratory in a chemical system, the connection between biology and Turing systems is still controversial. In [6] Kondo et al. showed that a Turing model could be matched with the stripe formation and addition on two different kinds of angelfish. The studies of angelfish have been extended by Varea et al. [7] and Painter et al. [8]. In Ref. [9] the role of boundary conditions have been investigated and as a result, a variety of patterns that bear striking resemblance to pigmentation patterns in fish are shown. A very recent paper by Barrio et al. [10] reviews the general properties of non-linear systems and how they can be utilized to describe a wide range of phenomena in many fields of Science.

Turing systems have also been applied in areas other than biology and chemistry. There is, of course, a huge amount of articles about applications of Turing systems in different fields, such as ecology [11], semiconductor physics [12, 13], material sciences [14, 15], hydrodynamics [16], astrophysics [17], optics [18] and even economics [19], to mention just a few. For a good review of applications of Turing systems especially in biology and chemistry the reader is encouraged to see the article by Maini [20] and references therein.

In this thesis the motivation is mainly theoretical (pattern formation) and we do not want to limit our models to some specific application. Our interest is in multi-layer systems but before we can actually study those we have to discuss about the background of the subject. Therefore, this thesis is organized as follows: First we will present some basic reaction diffusion models and examine their (linear) stability over the space of parameters. Models are illustrated with simulation results and, when appropriate, possible real-life examples are given. There is a short introduction to the numerical methods used in this thesis and a brief background of other mathematical tools used to analyze these systems. A short introduction for nonlinear analysis, namely dynamics, stability and amplitude equations, is also included. As an example,

we will show how to find the simplified amplitude equations for the BVAM model. More rigorous analysis is beyond the scope of this thesis and we shall refer to the literature whenever needed. It is presumed throughout that the reader possesses certain basic knowledge of partial differential equations of the kind studied here.

The last part of the thesis deals with the most recent research on the subject, namely multi-layer Turing systems. There has been a lot of interest in investigating ways of producing complex spatial patterns with Turing systems. One way of doing that consists of coupling several Turing systems linearly, such that the scales of the independent systems are well separated. This produces complicated superimposed patterns with different length scales. We will present, among others, the so called oscillatory Turing patterns (research carried out by I.R. Epstein et al.[21]). It includes models which consist of two- or multiple-layer systems. One of those models is very close to the well known Belousov-Zhabotinsky (BZ) reaction [22].

After reproducing the results published elsewhere [21], we examine the interesting case of *non-linearly* coupled Turing systems, where the intermediate layer also plays a role of setting new spatial scales, not present in the linear case. A more general model for coupled systems was proposed in [9] but in our case, the coupling will be symmetrical, and we shall treat the cubic and quadratic couplings separately. Our model is very similar to the linear case, in the sense that it preserves the location of the initial stable point allowing us to start with the same set of parameters as in the linear coupling and see what the nonlinear coupling brings into the scene. Extensive numerical simulations show that non-linear coupling generates a number of new regular patterns not observed in systems with linear coupling. Some of these patterns are superimposed patterns with different length scales. Furthermore, contrary to the linear case, the strength of the non-linear coupling is very important in the formation of the complex patterns. To our knowledge, no other studies have been carried out in this particular field.

Chapter 2

Reaction-Diffusion models

In this chapter we will briefly discuss the basic properties of reaction-diffusion models and pattern formation in Turing systems. To start with, we will discuss the basic features of the Turing instability, and then we will move on to some real applications. We will present a few well known reaction kinetics and show how they can be analyzed, mostly linearly though. A few definitions are also needed in order to understand when different instabilities occur, especially Turing and Hopf bifurcations. These equations and definitions are the tools that we use to find suitable parameters in the following chapters. In this thesis we will mostly neglect the non-linear analysis (see section 4.4.4) because it lies beyond the scope of this thesis. The main purpose of this chapter is to familiarize oneself with the basic mathematical background of the subject. Therefore, only few simulation results are shown.

This chapter is organized as follows: First we show a derivation of the general reaction-diffusion equations. Then we will show the general conditions for diffusion driven instabilities. The remaining part of this chapter is devoted to different kinds of reaction kinetics and their properties. The techniques are shown here in detail because they can be easily adapted to more complicated situations, as multi-layer systems.

2.1 Theory of pattern formation

Throughout this thesis we will study pattern forming systems that are described by a set of partial differential equations. They are called *reaction-diffusion equations* and one can write them formally in the following form:

$$\frac{\partial \mathbf{U}(\mathbf{r}, t)}{\partial t} = \mathbf{D} \nabla^2 \mathbf{U} + \mathbf{F}(\mathbf{U}, b), \quad (2.1)$$

where $\mathbf{U}(\mathbf{r}, t)$ is a vector whose components are the local concentration of chemicals, $\mathbf{F}(\mathbf{U}, b)$ represents the reaction kinetics, b is a set of control parameters that link the system with the external world, and \mathbf{D} is the matrix of diffusion coefficients. If $\mathbf{F} \equiv 0$ these equations reduce to a set of uncoupled diffusion equations, with well known behaviour. When \mathbf{F} is nonzero, the behaviour of the solutions can be highly complex, as we shall see later on. Although the number of the spatial dimensions of \mathbf{r} is not limited here, practical reasons usually force the maximum number of the spatial dimensions to be three¹.

The derivation of eq. (2.1) goes as follows: Let $c(\mathbf{x}, t)$ be the concentration of a specific chemical (morphogen) at point $x \in \mathbb{R}^3$ and time $t \in \mathbb{R}_+$. Consider an arbitrary domain $\Omega \subset \mathbb{R}^3$. Then, considering the conservation of matter, the rate of change of chemical in Ω is equal to its net production $f(\mathbf{u})$ minus the flux through the surface surrounding the domain:

$$\frac{d}{dt} \int_{\Omega} c d\Omega = - \int_{\partial\Omega} \mathbf{J} \cdot d\mathbf{S} + \int_{\Omega} f(\mathbf{u}) d\Omega \quad (2.2)$$

where \mathbf{J} is the flux of chemical c per unit area and $f(\mathbf{u})$ is net chemical production per unit volume. This can be modified using the divergence theorem² and then eq. (2.2) simplifies to

$$\int_{\Omega} \left(\frac{\partial c}{\partial t} + \nabla \cdot \mathbf{J} - f(\mathbf{u}) \right) d\Omega = 0 \quad (2.3)$$

This is true for all Ω if equation

$$\frac{\partial c}{\partial t} + \nabla \cdot \mathbf{J} - f(\mathbf{u}) = 0 \quad (2.4)$$

is satisfied. Next we use Fick's law, which states that

$$\mathbf{J} = -D \nabla c \quad (2.5)$$

¹Mainly because it's very difficult to visualize, say, four dimensions or more.

² $\int_{\Omega} \nabla \cdot \mathbf{J} d\Omega = \int_{\partial\Omega} \mathbf{J} \cdot d\mathbf{S}$

i.e. the chemical flux is proportional to the concentration gradient. Letting D_c be the diffusion coefficient for the specific chemical (assumed to be constant in Ω), and substituting (2.5) into (2.4), we finally get the desired result (2.1):

$$\frac{\partial c}{\partial t} = D_c \nabla^2 c + f(\mathbf{u}) \quad (2.6)$$

Now that we have the equation we can start analyzing it from a general point of view. In parametrically driven systems there could be two types of symmetry-breaking instabilities: the ones breaking time translation symmetry, leading to oscillations through a Hopf bifurcation, and the ones leading to spatial oscillations through a Turing bifurcation [23]. In this thesis we are mainly interested in the Turing's instability which, in a spatial reactor, will take place when a homogenous steady state becomes unstable to spatial perturbations with a finite wave number.

The linear analysis is a tool which can be used to determine the conditions for instabilities of the system and the critical wavelength. A detailed description of the method will be given in the next section. In case of a Turing instability, the critical wavelength only depends on intrinsic parameters such as rate constants and diffusion coefficients. The instability is driven by diffusion, and the nonlinear terms are responsible for stabilizing a spatial pattern. This is the reason why it is often called *diffusion driven instability*. Later on we will study systems where patterns can be obtained in different ways, either diffusion driven or not, by a proper selection of parameters.

Most of the physical phenomenology of Turing systems is found considering only two reacting chemicals u and v . The formation of a spatial pattern is only possible if the two chemicals fight each other to occupy the available space in the domain. These systems are usually called inhibitor-activator models, since one of the chemicals tends to intensify its own changes, while simultaneously, the inhibitor tries to oppose those changes. Due to that, a pattern can only arise when the local balance between these antagonist species is broken. Quite evidently this happens spontaneously when the diffusion coefficient of the inhibitor (D_u) is larger than that of the activator (D_v) or viceversa. Experience has shown, as Turing himself suggested, that in real applications the ratio $d = D_v/D_u$ has to be very different from one. When the roles of the activator and inhibitor are reversed, (the sign of the linearized jacobian determinant is minus one) the system is usually called cross activator-inhibitor.

In Ref. [4] a detailed analysis for general conditions for obtaining a diffusion-driven instability has been performed for a two-species reaction-diffusion mechanisms. In here we will only write these conditions as a reference. The

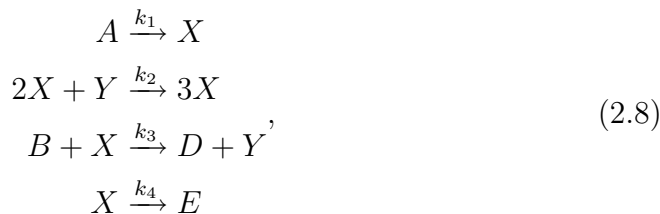
important thing is that these inequalities will give the boundaries for parameters resulting in a Turing instability. In the following expressions, the diffusion parameters D_u and D_v are replaced by the ratio d , because in these systems only the relative values matter. The inequalities now read as follows:

$$\begin{aligned}
 \partial_u f + \partial_v g &< 0 \\
 \partial_u f \partial_v g - \partial_v f \partial_u g &> 0 \\
 d \partial_u f + \partial_v g &> 0 \\
 (d \partial_u f + \partial_v g)^2 - 4d(\partial_u f \partial_v g - \partial_v f \partial_u g) &> 0
 \end{aligned} \tag{2.7}$$

where f and g are the two nonlinear reaction terms for u and v , respectively, and their partial derivatives with respect to the two variables are evaluated at the steady state \mathbf{w}_0 , where $\partial_t u = \partial_t v = 0$. It is evident that the first and the third inequalities imply that d must be different from one. When written in this form, these relations provide not only necessary, but also sufficient conditions for a diffusion driven instability.

2.2 Brusselator model

In this section we will present the Brusselator model and show the derivation of its well known equations 2.10. We also perform a linear stability analysis for this model. The Brusselator model was proposed by Ilya Prigogine (Nobel Laureate in Chemistry 1977) and co-workers in Brussels in 1971. The idea was to describe the autocatalytic oscillations ubiquitous in Nature, especially in the living bodies. The reaction equations for the model are:



where A and B are the reactants and X and Y are intermediate products while D and E are the final products, k_1, \dots, k_4 being the reaction rate constants. The evolution of the compounds X and Y is given by the equations:

$$\begin{aligned} \frac{dX}{dt} &= k_1 A + k_2 X^2 Y - k_3 B X - k_4 X \\ \frac{dY}{dt} &= -k_2 X^2 Y + k_3 B X \end{aligned} \quad (2.9)$$

Now we introduce dimensionless quantities and make the following transformations: $a = Ak_1/k_3$, $b = Bk_2/k_3$, $k_4 = k_3$, $X \rightarrow u$, $Y \rightarrow v$, $t \rightarrow tk_3$, $D_X/k_3 \rightarrow D_u$ and $D_Y/k_3 \rightarrow D_v$, then we have the desired Brusselator kinetics:

$$\begin{cases} \frac{du}{dt} = D_u \nabla^2 u + a - (b+1)u + u^2 v \\ \frac{dv}{dt} = D_v \nabla^2 v + bu - u^2 v \end{cases} \quad (2.10)$$

2.2.1 Linear analysis

Next, we will perform the linear stability analysis for the 2-dimensional reaction-diffusion model with the Brusselator kinetics. A detailed analysis will be done here with the help of the model introduced. This can be done without loss of generality, because the same techniques can be applied to other reaction-diffusion models as well. This can be seen in the forthcoming sections. We will also show a few general results of the stability analysis, which are independent of the model, side by side with the results for the Brusselator model. First of all, as we know the general form of a two-species reaction diffusion system is

$$\begin{cases} \frac{\partial u}{\partial t} = D_u \nabla^2 u + f(u, v) \\ \frac{\partial v}{\partial t} = D_v \nabla^2 v + g(u, v) \end{cases}, \quad (2.11)$$

where u and v are concentration fields of morphogens and f and g are non-linear functions that represent the reaction kinetics. The number of species (here two) has no limitations as can be seen in section 5, but when the number of equations increases, the mathematical analysis usually becomes more involved.

To formulate the problem mathematically we need, of course, initial and boundary conditions. In the simulations of this thesis, the initial condition is

usually a small random perturbation around the steady state $\mathbf{w}_0 = (u_0, v_0)$. This is partly due to the fact that the instability here is driven by diffusion. So if we start the simulation in each grid point in the vicinity of the steady state we will hopefully see how the diffusion drives the system to some non-uniform stable state. These stable states are patterns which can be seen later in this paper. Other initial conditions are also sensible. For instance, in cubic coupling (see Chap. 5) we took some other pattern as an initial state and examined how the system will react from this situation. In the last part of this thesis will see a system that bounces between two fixed points and as a result producing solitons.

The boundary conditions are more challenging because they can affect the solution (i.e. the pattern). If we are interested in self-organization of patterns, we do not want any external input (meaning zero flux on the boundary). If we would use fixed boundary conditions, the spatial pattern could be affected by the shape of the domain. When we chose to use periodic boundary conditions, the domain could be considered essentially infinite, and the pattern is self-organized. Therefore, throughout the simulations of this thesis we shall impose periodic boundary conditions. Briefly, these boundary conditions mean that if we have a closed domain $\Omega = [0, 1] \times [0, 1]$ then $\forall t \geq 0$

$$\begin{cases} u(0, y, t) = u(1, y, t), & \forall y \in [0, 1] \\ u(x, 0, t) = u(x, 1, t), & \forall x \in [0, 1] \\ v(0, y, t) = v(1, y, t), & \forall y \in [0, 1] \\ v(x, 0, t) = v(x, 1, t), & \forall x \in [0, 1] \end{cases} \quad (2.12)$$

The same can be formulated for higher dimensions (three or more). This boundary condition produces no surface effects and finite size effects can be ignored for all system sizes. However, this produces an artificial periodicity of the systems that one has to be aware of. With periodic boundary conditions, the square (or cubical in three dimensions) simulation box is replicated throughout space to form an infinite periodic lattice.

One can easily verify that the stationary state of the Brusselator model (Eq. 2.10) is

$$\mathbf{w}_0 = \begin{cases} u_0 = a \\ v_0 = \frac{b}{a} \end{cases} \quad (2.13)$$

The nonlinear part of equations 2.10 can be linearized by using Taylor series expansion (see for instance [24] and [25]) around the stationary point \mathbf{w}_0 :

$$\begin{cases} \frac{\partial u}{\partial t} = D_u \nabla^2 u + f(\mathbf{w}_0) + u \frac{\partial f}{\partial u} + v \frac{\partial f}{\partial v} + O(u^2, v^2, uv) \\ \frac{\partial v}{\partial t} = D_v \nabla^2 v + g(\mathbf{w}_0) + u \frac{\partial g}{\partial u} + v \frac{\partial g}{\partial v} + O(u^2, v^2, uv) \end{cases} \quad (2.14)$$

Notice that at the stationary point, both f and g are zero ($f(\mathbf{w}_0) = g(\mathbf{w}_0) = 0$) by definition. The idea behind the linear stability analysis is investigate the behaviour of the system very near the fixed point. This is fairly useful, as long as the the fixed point is not one of the so called borderline cases (center, star, degenerated node and non-isolated fixed point), see for instance [25]

In general, the solution of a linear first order equation is of the form

$$\mathbf{w}(\mathbf{x}, t) = \mathbf{w}^0 + \sum_j c_j e^{\lambda_j t} e^{-i\mathbf{k}_j \cdot \mathbf{x}}. \quad (2.15)$$

By substituting Eq. (2.15) into Eq. (2.14) one arrives at

$$|\mathbf{A} - \mathbf{D}k_j^2 - \lambda_j \mathbf{I}| = 0 \quad (2.16)$$

for each normal mode j . In the case of the Brusselator model, the jacobian matrix \mathbf{A} is

$$\mathbf{A} = \begin{pmatrix} \partial_u f & \partial_v f \\ \partial_u g & \partial_v g \end{pmatrix}_{\mathbf{w}_0} = \begin{pmatrix} b-1 & a^2 \\ -b & -a^2 \end{pmatrix} \quad (2.17)$$

Now, we have everything to write the characteristic equation. Remember that non-vanishing solutions exist only if the determinant (2.16) vanishes. Therefore, for each normal mode the characteristic equation gives a dispersion relation:

$$\begin{aligned} & \lambda^2 + [(D_u + D_v)k^2 - f_u - g_v]\lambda \\ & + D_u D_v k^4 - k^2(D_v f_u + D_u g_v) + f_u g_v - f_v g_u \\ & = \lambda^2 - \alpha \lambda + \beta = 0, \end{aligned} \quad (2.18)$$

where

$$\begin{cases} \alpha & = (-D_u - D_v)k^2 + b - a^2 - 1 \\ \beta & = a^2 + (a^2 D_u + D_v - b D_v)k^2 + D_u D_v k^4. \end{cases} \quad (2.19)$$

Solving eq. (2.18) with respect to λ yields

$$\lambda = \frac{\alpha \pm \sqrt{\alpha^2 - 4\beta}}{2}. \quad (2.20)$$

With the help of eq. (2.20) we can determine the stability of the system 2.10, but before that we need a few definitions.

Definition 2.2.1 (Hopf bifurcation theorem) ³ Consider a planar system of ordinary differential equations, written such a form as to make explicit the dependance on a parameter μ :

$$\begin{cases} \dot{x} &= f_1(x, y, \mu) \\ \dot{y} &= f_2(x, y, \mu) \end{cases} \quad (2.21)$$

Assume that this system has the origin as an equilibrium for all μ . Suppose that the linearization Df around zero has the two purely imaginary eigenvalues $\lambda_1(\mu)$ and $\lambda_2(\mu)$ when $\mu = \mu_c$. If the real part of the eigenvalues verify

$$\frac{d}{d\mu} = (\Re(\lambda_{1,2}(\mu)))|_{\mu=\mu_c} > 0 \quad (2.22)$$

and the origin is asymptotically stable at $\mu = \mu_c$, then μ_c is a bifurcation point.

Definition 2.2.2 (Turing instability) Turing instability occurs when ⁴:

$$\begin{cases} \Im(\lambda) = 0 \\ \Re(\lambda) > 0 \end{cases} \quad (2.23)$$

In this case, b could be chosen as the bifurcation parameter. So, for the Brusselator model the critical value of $b = b_c$ for a Hopf-bifurcation is

$$b > b_c^H = 1 + a^2, \quad (2.24)$$

³Also known as Poincaré-Andronov-Hopf theorem.

⁴ $\Im(x)$ is the imaginary part of x and respectively $\Re(x)$ is the real part of x .

and the Turing bifurcation occurs when [26]

$$b > b_c^T = \left(1 + a\sqrt{\frac{D_u}{D_v}}\right)^2. \quad (2.25)$$

According to [4] the critical wave number can be written as

$$k_c^2 = \frac{D_v f_u + D_u g_v}{2D_u D_v} = \sqrt{\frac{f_u g_v - f_v g_u}{D_u D_v}}, \quad (2.26)$$

where the notation is changed to $f_u = \partial_u f$ in all instances. Of course, the corresponding characteristic wavelength of the pattern is defined by $\lambda_c = 2\pi/k_c$.

Figure 2.1 shows the stability diagram of the spatially uniform steady state (SS) of the autonomous system in the (D_u, b) plane ($D_v = 1$). The Hopf bifurcation is the horizontal line (see Eq. (2.24)) and it crosses the Turing bifurcation line (see Eq. (2.25)) at $D_u = 5.19$. Figure 2.2 shows the dispersion curves at a few selected points (see [27]).

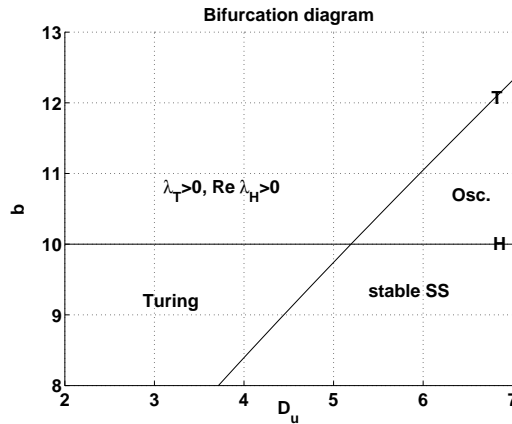


Figure 2.1: Bifurcation diagram. Hopf bifurcation: $b_c^H = 1 + a^2$; Turing bifurcation: $b_c^T = [1 + a\sqrt{D_u/D_v}]^2$, with fixed $a = 3$ and $D_v = 10$.

When equations 2.7 are applied to the Brusselator reaction kinetics one will end up to following inequalities:

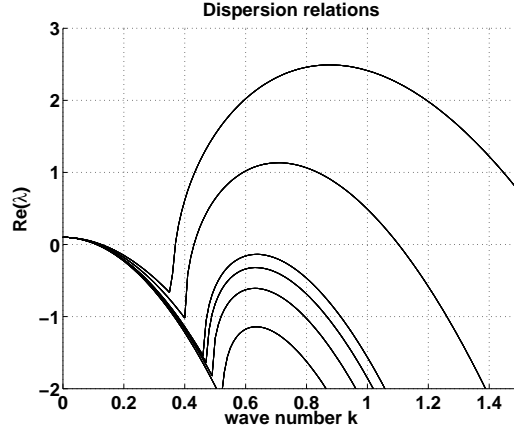


Figure 2.2: The real part of the dispersion relation with fixed $a = 3$ and with several values of D_v ($D_v = 10, 6.5, 6.0, 5.7, 5.5, 4.0, 2.5$)

$$\left\{ \begin{array}{l} f_u + g_v = -1 < 0 \\ f_u g_v + f_v g_u = a^2 - 2ba^2 > 0 \Rightarrow b < \frac{1}{2} \\ df_u + g_v = d(b-1) - a^2 > 0 \Rightarrow d \leq \frac{a^2}{1-b} \\ (df_u + g_v)^2 - 4d(f_u g_v - f_v g_u) \\ \quad = a^4 - 2a^2(b+1)d + (b-1)^2 d^2 > 0 \end{array} \right. \quad (2.27)$$

Finally, further analysis (see [4]) reveals that the necessary conditions for Turing instability are:

$$\begin{aligned} k_1^2 &= \frac{\gamma}{2d} \left[(df_u + g_v) - (df_u + g_v)^2 - 4d|A|^{1/2} \right] < k^2 \\ &< \frac{\gamma}{2d} \left[(df_u + g_v) + (df_u + g_v)^2 - 4d|A|^{1/2} \right] = k_2^2, \end{aligned} \quad (2.28)$$

where the interval (k_1, k_2) is known as the Turing region, γ is the relative strength of non-linear functions f and g , and $|A|$ is the determinant of the Jacobian matrix 2.17 (that is $|A| = f_u g_v - f_v g_u$). These equations give us the region of the linearly unstable wave-numbers that will produce Turing patterns.

We have illustrated that the benefit from this linear stability analysis is that it predicts the parameter values leading to some kind of instability (Turing,



Figure 2.3: Example of a stationary “labyrinthine” pattern obtained with the Brusselator model in a lattice of $s 256 \times 256$ and using the following parameters: $a = 3$, $b = 10.2$, $D_u = 4.0$, $D_v = 10$. The inset shows the Fourier spectrum of the pattern.

Hopf, ...). Furthermore, the characteristic length of the resulting pattern can be predicted effectively. However, there will be still a lot to discover, since linear analysis cannot predict the spatial mode selection made by the non-linear damping.

2.2.2 Simulation results

For the sake of completeness we show in Fig. 2.3 a typical pattern obtained numerically from this model in a 256×256 square lattice with periodic boundary conditions. We have also calculated its two-dimensional spatial Fourier spectrum, presented in the inset. This picture in k space is useful to detect at a glance the symmetries of the pattern. In this case we observe a circle that shows very clearly that the stripes have a very well defined wavelength, and no preferred orientation. Of course there is a huge amount of patterns, but in this paper, we are not so interested in these non-coupled models. The aim is to find out what happens when we couple these models (linearly, quadratically, or cubically). The parameters used in the figure can be found in the caption.

2.3 Gray-Scott model

The Gray-Scott model describes isothermal autocatalytic systems⁵ in the continuously flowing, well-stirred, tank reactor (CSTR). The model has great importance since it describes several experimentally observable autocatalytic reactions (for instance Ref. [28]: Belousov-Zhabotinskii reaction, Chorite-iodide-malonic acid reaction, arsenite-iodate reaction and Enzyme systems). The real reactions are rather complicated though, so to reduce the problem Gray and Scott focused on a model with overall stoichiometry.



The mass balance for this reaction is [28]

$$\begin{cases} \frac{da}{dt'} = -k_1ab^2 + k_f(a_0 - a) \\ \frac{db}{dt'} = k_1ab^2 - k_2b + k_f(b_0 - b) \end{cases}, \quad (2.30)$$

where k_1 , k_2 and k_f are reaction rates and a and b are the concentrations of the species (subscript 0 indicates the initial concentration respectively).

By using dimensionless quantities, i.e. u as the dimensionless reactant and v the dimensionless catalyst concentration and t as the dimensionless time, we will get

$$\begin{cases} \frac{\partial U}{\partial t} = D_U \nabla^2 U - UV^2 + F(1 - U) \\ \frac{\partial V}{\partial t} = D_V \nabla^2 V + UV^2 - (F + K)V \end{cases}, \quad (2.31)$$

where F and K are reaction parameters and D_U and D_V are the diffusion coefficients of the inhibitor and activator chemicals, respectively.

In the following we will find the steady states and perform a linear stability analysis very similarly as it was done in previous section for the Brusselator model. In the absence of diffusion $D_U = D_V = 0$, the steady state ($\frac{\partial U}{\partial t} = \frac{\partial V}{\partial t} = 0$) is generally attained at the point $(u, v) = (1, 0)$. Observe there are other two fixed points that are given by the following equations:

⁵Autocatalytic means that the catalyst is also the product

$$\begin{cases} u_{1,2} = \frac{1}{2} \left[1 \pm \sqrt{1 - 4 \frac{(F+K)^2}{F}} \right] \\ v_{1,2} = \frac{F}{2(F+K)} \left[1 \mp \sqrt{1 - 4 \frac{(F+K)^2}{F}} \right] \end{cases}. \quad (2.32)$$

This implies that these exist if $F \geq 4(F+K)^2$, meaning that the interior of the parabolic region is defined by $F = \frac{1}{2} \left[(1/4 - 2K) \pm \sqrt{1/16 - K} \right]$.

The point $(1, 0)$ is always stable. The stability of the other two points can be determined by the eigenvalues of the following matrix (see Eq. (2.17)):

$$\begin{aligned} \mathbf{A} &= \begin{pmatrix} -(F+v^2) & -2uv \\ v^2 & -(F+K)+2uv \end{pmatrix} \\ &= \begin{pmatrix} -(F+v^2) & -2(F+K) \\ v^2 & (F+K) \end{pmatrix}. \end{aligned} \quad (2.33)$$

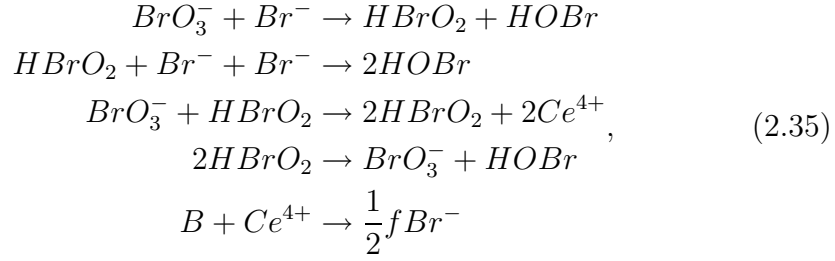
Now the determinant is $\Delta = (v^2 - F)(F + K)$ and the trace $\tau = -(v^2 - K)$. With these shorthand notations, the eigenvalues are

$$\lambda_{1,2} = \frac{1}{2} \left[\tau \pm \sqrt{\tau^2 - 4\Delta} \right]. \quad (2.34)$$

2.4 Oregonator model

The mechanism of the Belousov-Zhabotinsky Reaction was examined in the early 1970's by Richard M. Noyes, Richard J. Field, and Endre Koros at the University of Oregon. They proposed a model consisting of eighteen reactions and twenty-one distinct chemical species, resulting a system of rate equations (i.e. differential equations). The model considered here is a simplification of that: the Oregonator (its name origins from the University of Oregon). Although the model is a simplified version it still demonstrates the qualitative behaviour of the reaction. The Oregonator model gives the following steps⁶:

⁶ Br = bromine, O = oxygen, H = hydrogen, Ce = cerium. Do not confuse Br with B which is a shorthand notation for all oxidizable organic species present.



where B represents all oxidizable organic species present and f is stoichiometric factor that encapsulates the organic chemistry involved. When we introduce the following abbreviations

$$\begin{aligned}
A &\hookrightarrow BrO_3^- \\
B &\hookrightarrow \text{All oxidizable organic species} \\
P &\hookrightarrow HOBr \\
X &\hookrightarrow HBrO_2 \\
Y &\hookrightarrow Br^- \\
Z &\hookrightarrow Ce^{4+}
\end{aligned} \tag{2.36}$$

and change all the variables to dimensionless quantities, we will finally end up with the following system of differential equations (this derivation includes several steps, that are now omitted for simplicity)

$$\begin{cases} \frac{\partial x}{\partial t} = \frac{qy - xy + x(1-x)}{\epsilon} \\ \frac{\partial y}{\partial t} = \frac{-qy - xy + fz}{\epsilon'} \\ \frac{\partial z}{\partial t} = x - z \end{cases} . \tag{2.37}$$

where

$$\begin{cases} \epsilon = \frac{k_c B}{k_3 A} \\ \epsilon' = \frac{2k_c k_4 B}{k_2 k - 3A} \\ q = \frac{2k_1 k_4 B}{k_2 k_3 A} \end{cases} . \tag{2.38}$$

As a simulation result for this model, we will only show how the overall concentration of different chemical species oscillates with respect to time. Once it was thought that this kind of a behaviour is impossible. This model produces Turing patterns as well, but we will come back to those in section 5.2, where this model is applied to a realistic two-layer system. In Fig. 2.4 one can see a simulation of the system. The parameters and initial values are given in the caption of the figure.

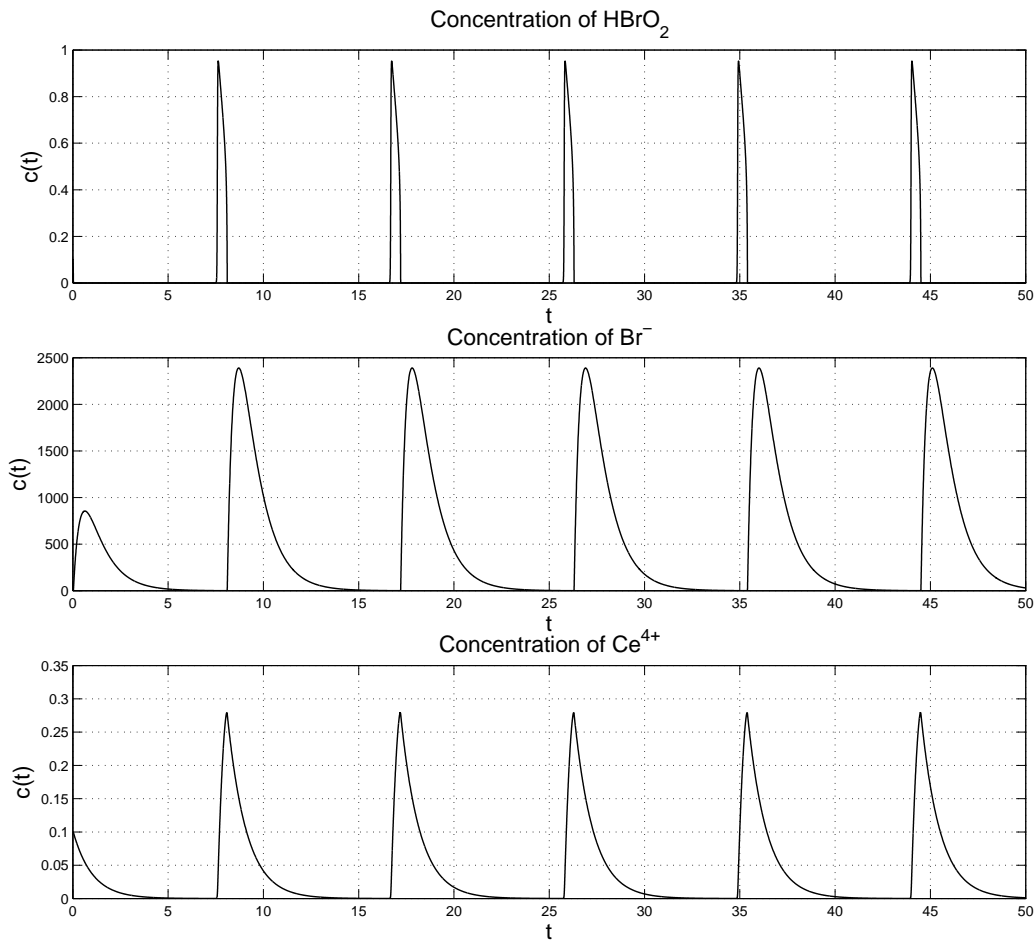
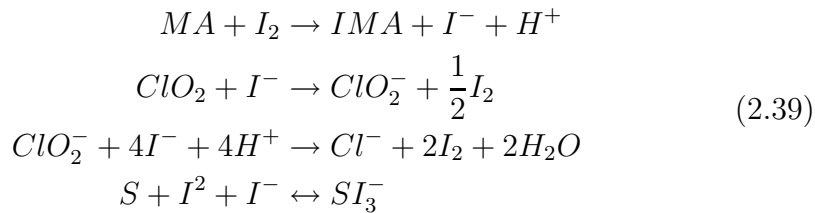


Figure 2.4: The relative concentrations of each species in a oscillatory Belousov-Zhabotinsky reaction. Parameters are: $A = 0.06, B = 0.02, f = 1, k_1 = 1.28, k_2 = 2.4 \cdot 10^6, k_3 = 33.6, k_4 = 3000$ and $k_c = 1$ and initial values are: $x_0 = 0.1, y_0 = 0$ and $z_0 = 0.1$

2.5 Lengyel-Epstein model

In the early 1950s the Russian biochemist Boris Belousov tried to mimic Krebs cycle (a metabolic process that takes place in living organisms). To his astonishment he found out that this chemical reaction oscillates (changed its color from yellow to colorless and to yellow again). Today, it is not a surprise that chemical reactions can oscillate, but in those days it was thought that all solutions of chemical reagents must go monotonically to equilibrium. Unfortunately he could not publish his radical discovery. Not until 1968 when a graduate student, Zhabotinsky, managed to confirm Belousov's observations and bring this work to light.

Later Istvan Lengyel, Gyula Rabai and Irving Epstein proposed a model for the oscillations in the chlorine-dioxide-iodine-malonic acid (CDIMA) reaction after the first experimental observation of a Turing pattern in 1989 in the chlorite-iodide-malonic acid (CIMA) reaction. In this thesis, we will only introduce the model and show a few basic results. Further analysis will not be performed although this model is important in sense that it captures the essential features of the CIMA reaction. For further information, especially of the photoresponse of CDIMA reaction, the reader is encouraged to see for instance Ref. [29]. The chemistry of the CDIMA reaction is represented by:



This leads to a five-variable model but with certain assumptions it can be reduced to a two-variable model. We will skip the derivation of this model and present its normalized equations:

$$\begin{cases} U_t = \frac{1}{\sigma} \left(\nabla^2 U + a - U - 4 \frac{UV}{1+U^2} \right) \\ V_t = d \nabla^2 V + b \left(U - \frac{UV}{1+U^2} \right) \end{cases}, \tag{2.40}$$

where a, b, d and σ are parameters that can be adjusted according to experimental reaction rates. Here, U and V are the dimensionless concentrations of I^- and ClO_2^- , respectively. The stationary state of this model is given by

$(U_0, V_0) = (a/5, 1 + a^2/25)$ and it has two types of bifurcations: The critical values for a Turing bifurcation are:

$$\begin{cases} b^T = \frac{d}{5a} \left(13a^2 - 4\sqrt{10}a\sqrt{25 + a^2} + 125 \right) \\ k_c = \sqrt{\frac{2\sqrt{10}a}{\sqrt{25 + a^2}}} - 5 \end{cases} \quad (2.41)$$

and for a Hopf bifurcation:

$$b^H = \frac{3a^2 - 125}{5a\sigma}. \quad (2.42)$$

2.6 Barrio-Varea-Aragon-Maini (BVAM) model

At the end of this chapter, we will introduce yet another model. This model has been introduced by Barrio et al. [9] and it has been studied extensively in [30]. Contrary to the previous models this one is based on no real chemical reactions but it is intended to be a general model, obtained by Taylor expanding the non-linear functions around the stable point, keeping terms up to third order, and respecting conservation laws, as the mass action rules. In the paper [9] this model was used to model the pattern formation on the skins of various fish species.

The model reads as follows:

$$\begin{cases} \frac{\partial u}{\partial t} = D\delta\nabla^2 u + \alpha u(1 - r_1 v^2) + v(1 - r_2 u) \\ \frac{\partial v}{\partial t} = \delta\nabla^2 v + \beta v(1 + \frac{\alpha r_1}{\beta} uv) + u(\gamma + r_2 v) \end{cases}, \quad (2.43)$$

where δ is a scaling factor, D is the ratio of diffusion coefficients of chemicals u and v , r_1 and r_2 are the non-linear parameters, and α , β and γ are the parameters for reaction kinetics. The equation (2.43) can be transformed to a more convenient form:

$$\begin{cases} \frac{\partial u}{\partial t} = D\nabla^2 u + \eta(u + av - Cuv - uv^2) \\ \frac{\partial v}{\partial t} = \nabla^2 v + \eta(bv + hu + Cuv + uv^2) \end{cases}, \quad (2.44)$$

where $a = 1/\alpha$, $b = \beta/\alpha$, $h = \gamma/\alpha$, $C = r_2/(\alpha\sqrt{r_1})$ and $\eta = L^2\alpha/\delta$. As it was noticed in [9], by the selection of parameter h , the number of stationary states can be controlled. If $h = -1$ ($\alpha = -\gamma$) we will have only one stationary point $\mathbf{w}_0 = (u_0, v_0) = (0, 0)$, but if $h \neq -1$ then we will have two other fixed points:

$$\mathbf{w}_0 = \begin{cases} v_0 = \frac{-C \pm \sqrt{C^2 - 4(h - b/g)}}{2}, \\ u_0 = -gv_0 \end{cases}, \quad (2.45)$$

where $g = (a + b)/(1 + h)$. Linear stability analysis when $h = -1$ can be carried out as usual and around the point $\mathbf{w}_0 = (0, 0)$. This yields a dispersion relation of the form:

$$\lambda^2 + \lambda[(1 + D)k^2 - \eta(1 + b)] + Dk^4 - \eta k^2(Db + 1) + \eta^2(b + a) = 0 \quad (2.46)$$

and by solving it, one obtains:

$$\lambda = \frac{1}{2}(-(1 + D)k^2 + \eta + b\eta \pm \sqrt{(D - 1)^2k^4 + 2(b - 1)(D - 1)k^2 + (-4a + (b - 1)^2)\eta^2}) \quad (2.47)$$

The general analysis is simplified if we omit the quadratic term, i.e. $C = 0$, because then $v_0 = \pm\sqrt{b/g - h} = \pm\sqrt{f}$.

In the paper by Barrio et al. [31] they noticed that Turing-like patterns could be produced even in absence of diffusion, when $h \neq -1$. This means that in this model there are interesting instabilities, other than diffusion driven ones.

2.7 Summary

In this chapter we have discussed the very basics of the theory of pattern formation and different reaction-diffusion models. We started with the derivation of the reaction-diffusion equation and then gave conditions for Turing instability. Next we moved to linear stability analysis which is a simple but effective tool for analysing reaction-diffusion systems. The last part of this

chapter was devoted to different reaction-diffusion models. All the models presented here are based on real, although simplified, reactions except the BVAM model which serves as a generic model. The most important model for this thesis is the one based on Brusselator kinetics since we use that in the coupled systems.

Chapter 3

Numerical methods

In this chapter we shall concentrate on numerical methods for solving the reaction-diffusion equations and other methods for analyzing the patterns. The first part concentrates on the discretization of the problem and numerical integration methods. Throughout this thesis we use a square lattice with periodic boundary conditions although, in nature, these patterns are formed usually on curved domains (see for instance Ref. [32]). The selection of the most appropriate integration method has to be done carefully, since low accuracy or numerical instability can easily lead to numerical artifacts and false conclusions. Thus we need to know the limitations of each method. In the second part, a few main results of Fourier-analysis are shown, which is one of the tools we need for analyzing the symmetries of the patterns.

3.1 Discrete time and solutions of differential equations

The general form of Turing system for two-species (or chemicals) reaction with periodic boundary conditions and an initial state is as follows:

$$\begin{cases} \frac{\partial u}{\partial t} = D_u \nabla^2 u + f(u, v) & , \quad \Omega = [0, L_x] \times [0, L_y] \\ \frac{\partial v}{\partial t} = D_v \nabla^2 v + g(u, v) \\ y(x_1, 0, t) = y(x_1, L_y, t) \\ y(0, x_2, t) = y(L_x, x_2, t) \\ y(x_1, x_2, 0) = g(x_1, x_2) \end{cases} \quad (3.1)$$

where $u \equiv u(\mathbf{x}, t)$ and $v \equiv v(\mathbf{x}, t)$ are the concentrations which depend on both time and space, and D_u and D_v are the respective diffusion constants. The functions f and g , that describe the reaction kinetics, as before, are typically non-linear.

Because the partial differential equations of the form (3.1) are usually very difficult or even impossible to solve in closed form (i.e. analytically) we have to use numerical methods, which require some kind of discretization of the problem. In the case of reaction-diffusion equations, we have to discretize both time and space. In all the simulations in this thesis, a rectangular lattice has been used. Of course, different domains can be used (circle/sphere, etc.), but to make things simple we chose a rectangular lattice. This is particularly convenient when using the finite difference method since the whole domain will be covered. For instance the finite element method is more effective method to solve such elliptic equations, especially in arbitrary shaped (if only convex) domains, but the implementation is more challenging and in our case not so useful. Of course, nowadays there are several commercial softwares available for this kind of problems, but here their use is not appropriate.

First of all we have to define a discretized version of the Laplacian operator $\nabla^2 = \Delta$, and in a two dimensional rectangular lattice it is written as follows

$$\nabla^2 y = \frac{\partial^2 y}{\partial x_1^2} + \frac{\partial^2 y}{\partial x_2^2}. \quad (3.2)$$

By approximating the derivatives twice and using a rectangular lattice, one obtains

$$\frac{\partial^2 y}{\partial x_1^2} \approx \frac{y_{i+1,j} - 2y_{i,j} + y_{i-1,j}}{h^2} \quad (3.3)$$

and similarly for $\frac{\partial y}{\partial x_2^2}$.

By repeating the process discussed above (remember periodic boundary conditions), one can write the discretized laplacian operator as $\Delta_h = I \otimes \Delta_{h_1} + \Delta_{h_2} \otimes I$, where

$$\Delta_{h_p} = \begin{pmatrix} -2 & 1 & \dots & 0 & 1 \\ 1 & -2 & \dots & 0 & 0 \\ \vdots & \ddots & \ddots & \ddots & \vdots \\ 0 & \dots & 1 & -2 & 1 \\ 1 & \dots & 0 & 1 & -2 \end{pmatrix}.$$

3.1.1 Euler Method

The next problem is to solve the time dependent partial differential equation. The simplest one is the famous Euler's (forward) method. Due the simplicity of the implementation we used it quite often or, when appropriate, substitute it with a more sophisticated version, called Improved Euler's method. Both of the algorithms start in the same way: Euler's method generates an approximate solution to the initial value problem

$$\begin{cases} y'(t) = f(t, y(t)) \\ y(t_0) = y_0 \end{cases} \quad (3.4)$$

In applications, $f(t, y(t))$ is a given function and t_0 and y_0 are the given initial values. Of course, the function $y(t)$ is the unknown one. By fixing the time step size h , we define the n :th time step as $t_n = t_0 + nh$ and arrive at Euler's method

$$\begin{cases} y_{n+1} = y_n + hf(t_n, y_n) + O(h^2) \\ y_0 = y(t_0) \end{cases} \quad (3.5)$$

The improved Euler also uses this as a trial step. The idea behind the improved version of the algorithm is that it approximates the integral at both ends of the interval. Therefore it is sometimes called the trapezoidal method (see Fig. 3.1). The exact area of this trapezoid is the length h of the base multiplied by the average of the heights of the two ends. With this, one obtains the Improved Euler's method;

$$\begin{cases} y(t_{n+1}) \approx y_{n+1} = y_n + \frac{1}{2} \left[f(t_n, y_n) + f\left(t_{n+1}, y_n + f(t_n, y_n)h\right) \right] h \\ y(t_0) = y_0 \end{cases} \quad (3.6)$$

3.1.2 Runge-Kutta Method

The Euler's (forward) method presented above is quite simple and, what is most important, it can be implemented very easily. Consequently, we have used this method to solve our differential equations. The method has anyhow its problems. First of all, the Euler's method is not very accurate compared to other, more sophisticated, methods run at the equivalent step size. Secondly,

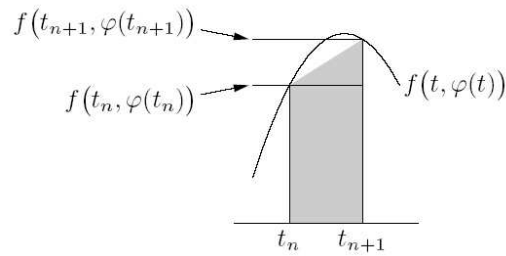


Figure 3.1: Improved Euler's method

the method is not very stable. Recall that the Euler's method is a first order method, that is the step error is $O(h^2)$ which means that the smaller the step size the smaller the error. In turn the smaller step size means longer the simulations. In our case the main problem arises when the systems show oscillations in time. If the oscillations are too rapid for the simple Euler, it will lead to numerical artifacts and therefore wrong conclusions. So, in brief, the motivation for the use of sophisticated methods should be obvious.

One of the major problems with the Euler's method (3.5) is that it is unsymmetrical: It advances the solution through an interval h , but uses derivative information only at the beginning of that interval. More or less the same way as it was done in previous section, we can construct a more symmetric integration method by making an Euler-like trial step to the midpoint of the interval, and then using the values of both x and y at the midpoint to make the real step across the interval. More precisely:

$$\begin{cases} k_1 = hf(x_n, y_n) \\ k_2 = hf(x_n + \frac{1}{2}h, y_n + \frac{1}{2}k_1), \\ y_{n+1} = y_n + k_2 + O(h^3) \end{cases} \quad (3.7)$$

where h is the step size. As indicated by the error term, this method is second order ¹ (in fact it is also known as the *second-order Runge-Kutta* or *midpoint* method) because the symmetrization cancels out the first-order error term. This is not the last word of this idea. We can evaluate the right-hand side $f(x, y)$ that all agree to first order, but that have different coefficients of higher-order error terms. Taking the right combination of these, will eliminate the error terms order by order. There are various specific formulas that emerge from this basic idea. We will now concentrate on the most often used classical *fourth-order Runge-Kutta formula*:

¹More generally, a method is called n th order if its error term is $O(h^{n+1})$.

$$\begin{aligned}
k_1 &= hf(x_n, y_n) \\
k_2 &= hf\left(x_n + \frac{1}{2}h, y_n + \frac{1}{2}k_1\right) \\
k_3 &= hf\left(x_n + \frac{1}{2}h, y_n + \frac{1}{2}k_2\right) \\
k_4 &= hf\left(x_n + \frac{1}{2}h, y_n + k_3\right) \\
y_{n+1} &= y_n + \frac{1}{6}k_1 + \frac{1}{3}k_2 + \frac{1}{3}k_3 + \frac{1}{6}k_4 + O(h^5)
\end{aligned} \tag{3.8}$$

The fourth-order Runge-Kutta method requires four evaluations of the right-hand side per step h . This should be superior to the midpoint method (3.7) for, at least, twice the step size with the same accuracy. Typically fourth-order Runge-Kutta is superior to second-order, but not always high order means high accuracy. From a physicist point of view, we shall be quite satisfied with that, and try to avoid abnormal cases whenever possible.

For our purposes, this method proved to be accurate enough, although there are numerous ways to improve this algorithm (i.e. adaptive step size, Cash-Karp parameters, etc.). In the case that some application requires better methods, we shall describe them then.

3.2 Fourier transform and structure factor

Fourier analysis (or harmonic analysis) is an extremely useful as a way to break up an arbitrary periodic function into a set of simple terms. A Fourier series, in basic form [33] reads as follows

$$f(x) = \frac{1}{2}a_0 + \sum_{n=1}^{\infty} a_n \cos(nx) + \sum_{n=1}^{\infty} b_n \sin(nx). \tag{3.9}$$

The Fourier transform is a generalization of the complex Fourier series in the limit $L \rightarrow \infty$ (i.e. the length of the interval goes to infinity). For further information about Fourier series, the reader is encouraged, for instance, to visit the Wolfram Research web site:

<http://mathworld.wolfram.com/FourierSeries.html>.

When the length of the interval is extended to infinity the sum (of sines and cosines) will become an integral

$$F(k) = \frac{1}{2\pi} \int_{-\infty}^{\infty} f(x) e^{-2\pi i k x} dx, \quad (3.10)$$

and the inverse transform is consequently

$$f(x) = \int_{-\infty}^{\infty} F(k) e^{2\pi i k x} dk. \quad (3.11)$$

In equations (3.10) and (3.11) k would refer to frequency and x to time (units $1/s$ and s) and the signal has a certain amplitude at a certain instant of time. In our case, there exists a certain concentration of substance at certain point \mathbf{r} . There might be time-dependent behaviour of the pattern, but we neglect that and investigate the spectrum at certain fixed instants. Thus we have space coordinates x (with unit m) so the Fourier transform will give us something like $1/m$. That is the wave vector \vec{k} . Now we can write the Fourier transform in convenient form as:

$$H(\vec{k}) = \int_{\Omega} h(\vec{x}) e^{i\vec{k}\cdot\vec{x}} d\vec{x} \quad (3.12)$$

where Ω refers to the d -dimensional spatial domain.

3.2.1 Discrete Fourier Transform

Our simulation results are not in continuous form, since the data are discrete sets. Therefore, we cannot simply use Eq. (3.10), but we have to discretize it, i.e. convert the integral to a sum. The definition of the (1-dimensional) discrete Fourier transform (DFT) is

$$F_n \equiv \sum_{k=0}^{N-1} f_k e^{-2\pi i k n / N}, \quad (3.13)$$

where N is the number of data points. The inverse transform is then

$$f_k = \frac{1}{N} \sum_{n=0}^{N-1} F_n e^{2\pi i k n / N}. \quad (3.14)$$

Basically Eq.(3.13) is enough, but it is very time consuming. Therefore there are several algorithms developed for this task. One of the most well known is the Fast Fourier Transform (FFT). It is an algorithm which reduces the number of operations for DFT provided $N = 2^m$. The number of operations needed using the definition is approximately N^2 whereas FFT needs only $N \log_2 N$ operations. There are many implementations of this algorithm so we do not have to build our own program for the task. The library we use is called FFTW, which stands for "Fastest Fourier Transform in the West". It is a free software developed at the Massachusetts Institute of Technology and can be found on their website <http://www.fftw.org/>.

3.2.2 Structure factor

In solid state physics structure factor is commonly used in determining the crystal structure. It represents the quantity related to the intensity of the reflection produced by the diffraction of coherent waves and it is independent of the method and conditions of observation. In X-ray crystallography the structure factor $F(hkl)$ of any X-ray reflection (diffracted beam produced by a collection of atomic planes indexed hkl) is the quantity that expresses both the amplitude and the phase of the diffraction phenomena. Researchers usually measure the structure factor of the material from X-ray or neutron scattering experiment. In general, the structure factor is the Fourier transform of a density matrix.

The static structure factor can be calculated from a pair correlation function $g(r)$. This is related to the probability of finding the center of a particle a given distance from the center of another particle. This is also known as the radial distribution function. For short distances $g(r)$ is related to the local packing of particles. Further away, these packing layers get more diffuse, and so for large distances, the probability of finding two spheres with a given density is essentially constant. Therefore, the static structure factor is defined as

$$S(k) = \int_0^\infty g(r) e^{ikr} dr. \quad (3.15)$$

In the present situation, we do not have atoms but concentrations i.e. a uniform scalar field over a certain domain. The structure factor of a Turing pattern should be calculated using, instead of the pair correlation function, one- and two-point correlation functions in the plane. This will change Eq. (3.15) to:

$$S(\vec{k}) = \int_0^\infty \sum_x (C_2(\vec{x}; \vec{x} + \vec{r}) - C_1^2(\vec{x})) e^{i\vec{k}\cdot\vec{r}} d\vec{r}. \quad (3.16)$$

This looks complicated, but the calculation is quite simple: First we subtract the average from the field in each point and then Fourier transform it. The Fourier transform converts the data from real space to the wave vector space. The structure factor can be then examined with respect to wave vector \vec{k} or wave number k .

3.2.3 Amplitude spectra

The information of the structure we require in this thesis can be obtained in a simpler way, by defining a Fourier spectrum of the concentration field. The Fourier spectrum can be calculated by using the equation

$$S(\mathbf{k}) = \sum_{i=1}^N (u(\mathbf{r}_i) - \bar{u}) e^{-i\mathbf{k}\cdot\mathbf{r}_i}, \quad (3.17)$$

where \bar{u} is the average concentration at a fixed time. One must notice that in our case the transform is two dimensional, but it turns out that it can be separated into a series of one-dimensional transforms. In other words, we transform each horizontal line of the pattern individually to yield an intermediate form in which the horizontal axis is frequency (f) and the vertical axis is space (v). We then transform individually each vertical line of this intermediate image to obtain each vertical line of the transformed image. Hence, a two dimensional transform of a $N \times N$ lattice consists of $2N$ one-dimensional transforms. We have not implemented the required algorithm in the computer, but we used the one provided in Matlab. It works as described above and it uses the FFTW library. The calculated spectrum is a matrix of complex numbers. The square of this quantity is called the power spectrum, and its square root, or its absolute value, is an amplitude spectrum. This gives us information about the amplitude of the modes in the two-dimensional k -space.

3.3 Summary

In this chapter the numerical methods used in this thesis, have been presented. First, the discretization transforming a continuous model to discrete

counterpart was described. Then we discussed different numerical integration methods and what are their weaknesses. It is important to note that careless use of these methods can lead to wrong results. The last part dealt with Fourier transform which will be used to find out the symmetry properties of the patterns.

Chapter 4

Analytical methods

After we have discussed about some numerical methods involved, it is time to move on to more analytical methods. The primary target of this chapter is to derive the amplitude equations at least in the simplest form. Before we deal with those equations we ought to discuss about some general features of pattern formation including dynamics, stability, bifurcations and other things. But, why do we need all this, rather than concentrate on the numerical solution of the equations? That is because, as mentioned several times already, linear analysis will not tell us much about the non-linear behaviour of the system and the non-linear behaviour is usually the most significant part of the pattern formation. Due to the demanding nature of this subject we shall not go deep into the details, but just introduce few ideas and examples of this kind of analysis. For further information of the subject reader is encouraged to see for instance [34] and references therein.

4.1 Dynamics and stability

In mathematics, stability theory deals with the stability of the solutions of differential equations and dynamical systems. The idea of stability is intuitive but it can be formulated mathematically. There are two different definitions for stability: Lyapunov stability and structural stability. In here we are interested in the first one, namely the Lyapunov stability criterion. In brief, if all trajectories in phase space that start near a point x stay near point x forever, then x is said to be *Lyapunov stable*. More strongly, if all points that start near point x converge to x , then x is *asymptotically stable*.

For continuous systems the definition can be formulated as follows: A system is said to be (uniformly) stable about a trajectory x “in the sense of

Lyapunov” if $\forall \epsilon > 0 \exists \delta > 0$ such that

$$\|y(t_0) - x(t_0)\| < \delta \quad (4.1)$$

which implies that

$$\|y(t) - x(t)\| < \epsilon \quad (4.2)$$

$\forall t \in \mathbb{R}^+$ and where the norm $\|\cdot\|$ is defined in the phase space. If in addition

$$\|y(t) - x(t)\| \rightarrow 0 \quad (4.3)$$

holds for $t \rightarrow \infty$, then trajectory x is (locally) *attractive*. If this property holds for all trajectories, then it is *globally attractive*. If x is both, attractive and stable, then it is said to be *asymptotically stable*¹. The definition for discrete-time systems is almost identical.

In this thesis we are mostly interested in systems where the kinetics can be described by a set of equations of the form

$$\frac{dx_n}{dt} = f_n(\mathbf{x}, \theta) \quad (4.4)$$

where $\mathbf{x} = (x_1, \dots, x_n)$ is a vector for the n species, θ holds for the control parameters and all the f_n 's are usually nonlinear functions of the species and parameters. Let the equilibrium point of the system be $\bar{\mathbf{x}}$, ie. $f(\bar{\mathbf{x}}) = 0$. Now, how we can determine the stability or instability of $\bar{\mathbf{x}}$ (in the sense of Lyapunov)? He introduced two main methods: The first is Lyapunov's *first* or *indirect* method, and the second, is called Lyapunov's *second* or *direct* method. We have already used the first method without mentioning it, but let us show it here again in a more general form. We start with the nonlinear system as in Eq.(4.4) and Taylor expand it around point $\bar{\mathbf{x}}$ (let's also redefine $\mathbf{x} \rightarrow \mathbf{x} - \bar{\mathbf{x}}$).

$$\frac{d\mathbf{x}}{dt} = \mathbf{A}(\mathbf{x}) + g(\mathbf{x}) \quad (4.5)$$

where \mathbf{A} is the Jacobian of the system evaluated at point \mathbf{x} and $g(\mathbf{x})$ contains the higher order terms, i.e.

¹ Notice that being attractive does not imply asymptotic stability

$$\lim_{|\mathbf{x}| \rightarrow 0} \frac{|g(\mathbf{x})|}{|\mathbf{x}|}. \quad (4.6)$$

Then, the nonlinear system (4.4) is asymptotically stable if, and only if, all the eigenvalues of A have negative real parts. The stationary states, or fixed points, can be classified further according to the imaginary parts and signs of the corresponding eigenvalues. For a more detailed discussion of the stability of fixed points, see, for instance, Ref. [35].

This method is very popular because it is easy to use and it works well with most of the systems. All we need is to be able to evaluate partial derivatives. On the other hand, if some of the eigenvalues of A are zero and others have negative real parts we cannot draw any conclusions about the stability of the nonlinear system. So the stable point $\bar{\mathbf{x}}$ can be either stable or non-stable. An other disadvantage of this method is the linearization. Therefore it is valid only when the initial conditions are close to a stable point.

An alternative method is a generalization of Lagrange's concept of stability of a minimum potential energy. If there is a function, called Lyapunov function $V(\mathbf{x})$, which has following properties:

1. $V(\bar{\mathbf{x}}) = 0$
 2. $V(\mathbf{x}) > 0, \quad \forall \mathbf{x} \neq \bar{\mathbf{x}}$
 3. $\dot{V}(\mathbf{x}) < 0$ along trajectories of $\dot{\mathbf{x}} = f(\mathbf{x})$
- (4.7)

Then $\bar{\mathbf{x}}$ is asymptotically stable. This method hinges on the existence of a Lyapunov function. It should be noticed that the derivative $\dot{V}(\mathbf{x})$ is considered to be a total differential along the solution curves of $\dot{\mathbf{x}} = f(\mathbf{x})$. Although this second method is very powerful and it has certain advantages, compared to the first one, we refrain from using it, because in some of our applications the Lyapunov potential function does not exist.

4.2 Bifurcations

In the previous section we discussed about stability and how it can be examined. Here we will discuss about another basic concept of pattern formation, namely bifurcations. In short, bifurcation refers to a qualitative change in the dynamics of a system and the parameter values at which they occur are called bifurcation points. Bifurcation is closely connected with stability, i.e. when a system goes through a bifurcation, a new set of stationary states (or fixed points) appear, which means that the stability of the stationary states

changes. Bifurcations are important because they are a universal feature of nonlinear systems, and they provide models of transitions and instabilities as some control parameter is varied. For instance, imagine a small weight placed on top of a beam. When the weight is small, the beam is able to support the load and remain vertical. But if the weight of the load is increased, at some point the load is too heavy and the beam bends. Then, the vertical position becomes unstable, and there is a set of new stable points, namely the bent positions at arbitrary azimuthal angle. In this example the bifurcation parameter is simply the weight of the load. This example is called the Zeeman machine. In general, the linearly stable point (the vertical in this case) is more symmetric than the new stable points after the bifurcation, then one recognizes that *symmetry breaking* is also a universal feature of nonlinear behaviour.

There are many types of bifurcations. For instance, a supercritical pitchfork bifurcation took place in the previous example (the beam and the load) when the only stationary point lost stability and two new stationary states appeared (when the beam is flat as a ribbon, and bends either to the left or to the right). Other examples of bifurcations are saddle-node bifurcations, transcritical bifurcations and Hopf bifurcations. Their names refer to different kinds of changes in the topology of the phase space. They can be further classified as subcritical ² and supercritical ³ depending on the direction of the bifurcation. A further classification on the co-dimension of the bifurcation which counts the number of control parameters for which fine tuning is necessary in order to get such a bifurcation. Saddle-node bifurcations are the only generic local bifurcations which are really co-dimension one, others have higher co-dimension. On the other hand, also pitchfork and transcritical bifurcations are sometimes considered as co-dimension one bifurcations because of their normal forms ⁴.

The bifurcations can be analyzed based on the eigenvalues and the eigenvectors determined by the linear stability analysis around some stationary point. If there is an eigenvalue with zero real part a local bifurcation occurs. If the eigenvalue is equal to zero, the bifurcation is a steady state bifurcation and if the eigenvalue is non-zero but purely imaginary, then the bifurcation is a Hopf bifurcation. The eigenvectors span the stable ($\lambda_i < 0$) and unstable ($\lambda_i > 0$) subspaces. When the system loses stability, the number of eigenvalues and eigenvectors associated with this change, is typically small. Therefore in such systems the linearization typically has a very large stable part and a small number of critical modes which change from stable to un-

² The branch of solutions occurs for parameter values on the *opposite* side of the loss of stability. Often indicates that the new branch is *unstable*.

³The branch of solutions occurs for parameter values on the *same* side as the loss of stability. Often indicates that the new branch is *stable*.

⁴Normal form means the simplest differential equation that captures the essential features of a system near a bifurcation point.

stable as the bifurcation parameter exceeds the critical value. The idea of center manifold theorem is based on the observation that near the onset of instability the dynamics of the system is governed by these critical modes and the stable modes just “follow” in passive fashion. The center manifold theorem allow us to reduce the problem into a smaller, manageable one.

The dynamics on center manifold is described by normal forms or amplitude equations. They are universal in the sense that all systems showing certain bifurcation have the same dynamics on the center manifold. We will not go any deeper in this subject but we refer the reader for more information to Ref. [36, 37]. Last, it is worth mentioning the fact that a *Turing bifurcation* is different from other bifurcations discussed here. In brief, during a Turing bifurcation the number of stationary states does not change but a stationary state in the absence of diffusion, becomes unstable when diffusion is allowed, leading to a *Turing instability*. In the case of reaction-diffusion systems this means that stationary patterns will rise spontaneously starting from arbitrary initial configuration. The key factor is the diffusion and therefore Turing instability is most often referred as *diffusion-driven instability*.

4.3 Complex Ginzburg-Landau equation

The complex Ginzburg-Landau equation (CGLE) is one of the most-studied equations in applied mathematics. It describes qualitatively, and often quantitatively, a vast array of phenomena, including nonlinear waves, second-order phase transitions, Rayleigh-Bénard convection and superconductivity. The equation describes the evolution of amplitudes of unstable modes for any process exhibiting a Hopf bifurcation, for which a continuous spectrum of unstable wave numbers is taken into account. It can be viewed as a highly general normal form for a large class of bifurcations and nonlinear wave phenomena in spatially extended systems. Here we will concentrate on the the use of CGLE in pattern formation theory and especially in reaction-diffusion systems.

In pattern formation theory the CGLE describes the dynamics of generic spatially extended systems which undergo a supercritical Hopf bifurcation from a stationary state to an oscillatory state. With the classical reductive perturbation method, any reaction-diffusion system that is close to the onset of this bifurcation, can be described by the complex Ginzburg-Landau equations. The cubic form is:

$$\partial_t A = A + (1 + i\alpha)\nabla^2 A - (1 + i\beta)|A|^2 A \quad (4.8)$$

where A is the complex amplitude of the oscillation, i is the imaginary unit, and α and β are adjustable parameters. The CGLE shows the typical wave solutions (plane, spiral, target), but also localized coherent structures and even spatio-temporal chaotic behaviour. Due to its generic nature the CGLE is most probably the most studied of all reaction-diffusion models. For deeper understanding of the CGLE, the reader is encouraged to look for instance Ref. [34].

As a curiosity, we show at the end of this section a developed version of CGLE when there is periodic forcing present. This is called *Forced Complex Ginzburg-Landau equation* (FCGLE) and it has been derived by Lingfa et al. The derivation can be found from the appendix A.1. This can be used to analyze oscillatory Turing patterns under periodic forcing as it was done by Epstein et al. in [27]. The FCGLE equation is as follows:

$$\frac{\partial A}{\partial t} = (\mu + i\nu)A - (1 + i\alpha)|A|^2A + (1 + i\beta)\nabla^2 A + \gamma A^* \quad (4.9)$$

where other parameters are the same as in the normal CGLE, except that μ represents the distance from the Hopf bifurcation, $\nu = \Omega - \omega_f/2$ is the detuning frequency shift and γ is the forcing amplitude.

4.4 Amplitude equations

As we have noticed in general, nonlinear equations cannot be solved analytically. Therefore, the behaviour of the patterns have to be explained by other means. The amplitude equations method is one of the most efficient ways to do that, because they describe slow modulations in space and time of a simple basic pattern. One notable thing is that the form of these equations does not depend on the details of the underlying system. The particular physical details are taken into account by the coefficients. Due to the demanding nature of this subject, we have to rely on the literature. Therefore, most of the derivation here has been taken from Ref. [38] and [39]. The idea of the remaining part of this chapter is to show the reader what the amplitude equations look like and what can be said on the basis of them. The derivation of the equations here is far beyond the scope of this thesis except for the simplest form in the BVAM model.

4.4.1 Introduction to perturbation theory

The idea of perturbation theory is to find an approximate solution to a problem that cannot be solved exactly. First, we start with a simpler system which can be solved analytically, and then turn on additional “disturbance”. This theory is applicable if the original problem can be formulated by adding a small term to the mathematical description of the exactly solvable problem.

Perturbation theory leads to an expression for the desired solution in terms of a power series with some small parameter that quantifies the deviation from the exactly solvable problem. The leading term in this series is the solution for the exactly solvable system and the other terms describe the deviations of the solution due to the differences with the initial problem. Formally, this looks like:

$$A = A_0 + \varepsilon A_1 + \varepsilon^2 A_2 + \dots \quad (4.10)$$

Here A is the full solution, A_0 is the solution for the simplified problem and the other, higher order, terms are obtained by some iterative process. If the deviation parameter ε is small, the higher order terms become less important and they can be neglected at some point.

4.4.2 Square Turing patterns

In this section we show the amplitude equations for square Turing patterns and in the next section for hexagonal patterns. Most of the derivation is missing but the idea is only to show the results and discuss a little about them. For those who are interested we encourage to see for instance Ref. [30], where nonlinear bifurcation analysis is done rigorously.

Square lattices are formed by two perpendicular vectors \mathbf{k}_1 and \mathbf{k}_2 . The field vector is presented by

$$c(\mathbf{r}, t) = A_1 e^{i\mathbf{k}_1 \cdot \mathbf{r}} + A_2 e^{i\mathbf{k}_2 \cdot \mathbf{r}} + \bar{A}_1 e^{-i\mathbf{k}_1 \cdot \mathbf{r}} + \bar{A}_2 e^{-i\mathbf{k}_2 \cdot \mathbf{r}}. \quad (4.11)$$

Then, the cubic amplitude equations are of the form:

$$\begin{aligned} \tau_0 \frac{\partial A_1}{\partial t} &= [\mu - (g_1 A_1^2 + g_2 A_2^2)] A_1 \\ \tau_0 \frac{\partial A_2}{\partial t} &= [\mu - (g_1 A_2^2 + g_2 A_1^2)] A_2 \end{aligned} \quad (4.12)$$

To split the real and imaginary parts, let $A_i = \rho_i e^{i\varphi_i}$ and substitute this into Eq. (4.12). Then, the modulus equations can be obtained. The stabilities of the three stationary solutions can be determined by the eigenvalues of the Jacobian matrix:

$$J(\rho_1, \rho_2) = \begin{bmatrix} \mu - 3g_1\rho_1^2 - g_2\rho_2^2 & -2g_2\rho_1\rho_2 \\ -2g_2\rho_1\rho_2 & \mu - 3g_1\rho_2^2 - g_2\rho_1^2 \end{bmatrix} \quad (4.13)$$

The trivial solution is, of course, $\rho_1 = \rho_2 = 0$ and then the eigenvalues are $\lambda_{1,2} = \mu$. This is stable when $\mu < 0$.

One stripe solution occurs when $\rho_1 = \sqrt{\mu/g_1}$ and $\rho_2 = 0$. Then the eigenvalues are

$$\begin{aligned} \lambda_1(\mu) &= -2\mu \\ \lambda_2(\mu) &= \mu \left(1 - \frac{g_2}{g_1} \right) \end{aligned} \quad (4.14)$$

Then the stability conditions are respectively: $\mu > 0$ and $g_2/g_1 > 1$.

The third solution is a square lattice, when $\rho_1 = \rho_2 = \sqrt{\mu/(g_1 + g_2)}$. Now the eigenvalues are

$$\begin{aligned} \lambda_1(\mu) &= -2\mu \\ \lambda_2(\mu) &= -2\mu \frac{g_1 - g_2}{g_1 + g_2} \end{aligned} \quad (4.15)$$

and the conditions for stability are: $\mu > 0$ and $-1 < g_2/g_1 < 1$.

4.4.3 Hexagonal Turing patterns

Simple hexagonal lattices are formed by resonant triplets of vectors $\mathbf{k}_1 + \mathbf{k}_2 + \mathbf{k}_3 = 0$ with rotational symmetry $|\mathbf{k}_1| = |\mathbf{k}_2| = |\mathbf{k}_3| = k_c$. The concentration field can be described by three amplitudes A_i and their complex conjugates:

$$c(\mathbf{r}, t) = A_1 e^{i\mathbf{k}_1 \cdot \mathbf{r}} + A_2 e^{i\mathbf{k}_2 \cdot \mathbf{r}} + A_3 e^{i\mathbf{k}_3 \cdot \mathbf{r}} + c.c. \quad (4.16)$$

The cubic amplitude equations are:

$$\begin{cases} \tau_0 \frac{\partial A_1}{\partial t} = \mu A_1 + h \bar{A}_2 \bar{A}_3 - [g_1 A_1^2 + g_2 (A_2^2 + A_3^2)] A_1 \\ \tau_0 \frac{\partial A_2}{\partial t} = \mu A_2 + h \bar{A}_3 \bar{A}_1 - [g_1 A_2^2 + g_2 (A_3^2 + A_1^2)] A_2 \\ \tau_0 \frac{\partial A_3}{\partial t} = \mu A_3 + h \bar{A}_1 \bar{A}_2 - [g_1 A_3^2 + g_2 (A_1^2 + A_2^2)] A_3 \end{cases} \quad (4.17)$$

In order to split the real and imaginary parts let us define, as before $A_i = \rho_i e^{i\varphi_i}$. One phase equation reads then

$$\tau_0 \frac{\partial \phi}{\partial t} = -h \frac{\rho_1^2 \rho_2^2 + \rho_2^2 \rho_3^2 + \rho_3^2 \rho_1^2}{\rho_1 \rho_2 \rho_3} \sin \varphi \quad (4.18)$$

Now the three modulae equations read:

$$\begin{cases} \tau_0 \frac{\partial \rho_1}{\partial t} = \mu \rho_1 + p \bar{\rho}_2 \bar{\rho}_3 - [g_1 \rho_1^2 + g_2 (\rho_2^2 + \rho_3^2)] \rho_1 \\ \tau_0 \frac{\partial \rho_2}{\partial t} = \mu \rho_2 + p \bar{\rho}_3 \bar{\rho}_1 - [g_1 \rho_2^2 + g_2 (\rho_3^2 + \rho_1^2)] \rho_2 \\ \tau_0 \frac{\partial \rho_3}{\partial t} = \mu \rho_3 + p \bar{\rho}_1 \bar{\rho}_2 - [g_1 \rho_3^2 + g_2 (\rho_1^2 + \rho_2^2)] \rho_3 \end{cases} \quad (4.19)$$

This has five stationary solutions: one trivial uniform solution, one with stripes, two hexagonal solutions and one mixed mode solutions. These can be analysed similarly as in the previous section by writing the Jacobian and solving for its eigenvalues.

4.4.4 Amplitude equations for BVAM-model

Here, we will derive the amplitude equations for the BVAM-model described in Sect. 2.6. The actual work has been done elsewhere [31] and we just show here the derivation. A similar method can be used to find the equations for other systems, as long as we are aware of the limitations of the perturbation theory.

The derivation goes as follows. First the reaction diffusion equations are:

$$\begin{cases} \frac{\partial u}{\partial t} = D\nabla^2 u + \alpha_{11}u + \alpha_{12}v - uv^2 \\ \frac{\partial v}{\partial t} = \nabla^2 v + \alpha_{21}u + \alpha_{22}v + uv^2 \end{cases} \quad (4.20)$$

In Ref. [31] the diffusion coefficient ratio is set to $D = 1$, for simplicity. Next, we will take a grid of size $N \times N$. This is quite obvious since in all of the simulations we have used a rectangular lattice. However, there is no loss of generality, because other domains are also possible to deal with similar techniques (see for instance [40] and references therein). For the sake of simplicity, we will take a rectangular grid. The possible modes have a wave number

$$k = \frac{2\pi}{N}n, \quad n \in \mathbb{Z} \quad (4.21)$$

Then, the solution of (4.20) can be cast in the form

$$\begin{cases} u(\mathbf{x}, t) = \sum_{n=1}^N \left(A_n(t)e^{i\frac{2\pi}{N}n} + A_{-n}(t)e^{-i\frac{2\pi}{N}n} \right) \\ v(\mathbf{x}, t) = \sum_{n=1}^N \left(B_n(t)e^{i\frac{2\pi}{N}n} + B_{-n}(t)e^{-i\frac{2\pi}{N}n} \right) \end{cases} \quad (4.22)$$

where A_n , A_{-n} , B_n and B_{-n} are the time dependent coefficients of the amplitudes. Next, Eq. (4.22) will be substituted into Eq. (4.20), then multiplied by $e^{-i\frac{2\pi}{N}L}$ and integrated over $x = L/N$.

So far it has been quite straightforward, but now one has to make approximations. If we solve all the coefficients of eq. (4.22), we will get the exact solution. However, this is not possible in general, because there are (or there might be) an infinite number of coefficients. Here, we apply the main idea of perturbation theory (see section 4.4.1), that is to find an approximative solution for the differential equation when the system is set very near to a known solution. Therefore, due to the quantized nature of the modes confined in a finite domain (see Eq. 4.21, and with the observation that the dispersion relation predicts eigenmodes with positive real part near the origin, we can set the parameters to pump only two modes in a marginal way, allowing us to truncate the series of Eqs. (4.22), retaining only the first two coefficients. The only two modes which can be pumped up are K_1 and $K_3 = 3K_1$. That is, the center manifold contains only these two modes, and they govern the long time dynamical behaviour of the nonlinear system.

Now we are ready to solve for the amplitudes. The linear terms are straightforward, by assuming even solutions, i.e.

$$\begin{cases} A_1 = A_{-1} \\ A_3 = A_{-3} \\ B_1 = B_{-1} \\ B_3 = B_{-3} \end{cases}, \quad (4.23)$$

where the indices indicate one of the two pumped modes. The cubic terms are more challenging:

$$\begin{aligned} \sum_L e^{-i\frac{2\pi}{N}L} uv^2 &= \sum_L \sum_{n,m,l} A_n B_m B_l e^{i\frac{2\pi}{N}(n+m+l-L)} = \\ &= \sum_{nml} A_n B_m B_l \delta_{(n+m+l,L)} = \sum_{n,m} A_n B_m B_{L-n-m} \end{aligned} \quad (4.24)$$

which implies that $l = L - m - n$. Then

$$\begin{cases} n, m = \pm 1, \pm 3 \\ L = \pm 1, \pm 3 \end{cases} \quad (4.25)$$

Now if we, for instance, choose $n, m > 0$ we will get the following terms:

$$\begin{aligned} &\sum_{L=\pm 1, \pm 3} (A_1 B_1 B_{L-2} + A_1 B_3 B_{L-4} + A_3 B_1 B_{L-4} + A_3 B_3 B_{L-6}) \\ &= A_1 B_1 B_{-1} + A_1 B_1 B_1 + A_1 B_1 B_{-3} + A_1 B_1 B_{-5} \\ &\quad + A_1 B_3 B_{-3} + A_1 B_3 B_{-5} + A_1 B_3 B_{-1} + A_1 B_3 B_{-7} \\ &\quad + A_3 B_1 B_{-3} + A_3 B_1 B_{-5} + A_3 B_1 B_{-1} + A_3 B_1 B_{-7} \\ &\quad + A_3 B_3 B_{-5} + A_3 B_3 B_{-7} + A_3 B_3 B_{-3} + A_3 B_3 B_{-9} \end{aligned} \quad (4.26)$$

Then, one makes $B_a = 0$ for $a \neq \pm 1, \pm 3$ and $B_a = B_{-a}$ and collects (linear and cubic) terms. One finally arrives at the following amplitude equations:

$$\begin{aligned}
\frac{dA_1}{dt} &= (1 - k^2)A_1 + g(1 - f)B_1 \\
&\quad - (3A_1B_1^2 + 4A_3B_1B_3 + A_3B_1^2 + 2A_1B_1B_3 + 2A_1B_3^2) \\
\frac{dB_1}{dt} &= [g(h + f) - k^2]B_1 + hA_1 \\
&\quad + 3A_1B_1^2 + 4A_3B_1B_3 + A_3B_1^2 + 2A_1B_1B_3 + 2A_1B_3^2 \\
\frac{dB_3}{dt} &= (1 - 9k^2)A_3 + g(1 - f)B_3 \\
&\quad - (A_3B_1^2 + 4A_1B_1B_3 + 3A_3B_3^2 + 2A_3B_1^2) \\
\frac{dB_3}{dt} &= [g(h + f) - 9k^2]B_3 + hA_3 \\
&\quad + A_3B_1^2 + 4A_1B_1B_3 + 3A_3B_3^2 + 2A_3B_1^2
\end{aligned} \tag{4.27}$$

These equations can be solved numerically, and give information about the nature of the pattern in k space.

4.5 Summary

In this chapter we focused on (weakly) non-linear analysis, because in order to get deeper understanding to the dynamics of the reaction-diffusion systems one has to go beyond linear analysis. The bifurcations are closely related to stability since they tell how the dynamics (i.e. stability and the number of the stable points) changes. Then we moved on to complex Ginzburg-Landau equation which led us to amplitude equations. These equations tell us what sort of patterns we are going to have and how they evolve as the time goes by. As an example we showed the equations for square and hexagonal Turing patterns and we also showed the derivation for the amplitude equations for the BVAM-model in detail.

Chapter 5

Coupled Turing Systems

In this chapter we will extend our study of reaction-diffusion systems. As mentioned earlier, the whole idea of Turing systems was to explain pattern formation in some real chemical and biological systems. However, in order to mimic real systems, it should be recognized that more complicated models, either with more morphogens or by introducing more complex interactions, are needed. For this purpose, it was proposed few years ago that coupling two simple Turing systems could produce more complex patterns and could simulate reasonably well some complicated structures, e.g. the skin coats of some fish species [9, 41]. There linear, quadratic and cubic couplings were used, and it was found that linear and cubic terms could modify the basic stripe or spot patterns substantially, contrary to quadratic coupling that had very little effect on the basic patterns.

More recently, there has been a series of interesting papers investigating a way of linearly coupling two sets of Turing equations using the Brusselator model [21], the Oregonator model [22], or the Lengyel-Epstein model [42]. All these models preserve the stable fixed point in the absence of diffusion, and when the parameters ensure unstable resonating modes for two different wavelengths, beautiful patterns appear. As results one can obtain complex superimposed patterns, for instance spots contained in stripes or vice versa, or patterns with spots of two different sizes (wavelengths), and a whole variety of other complicated patterns. These models could be interpreted as systems consisting of two chemically active layers, separated by an intermediate layer that is not chemically active, but allows transport of chemicals through it. Real experimental research has been carried out in this particular field of multilayered systems (see [43]).

These models can also be used to describe semiconductor bilayer systems or even more complicated systems as biological membranes. Since there are situations in which the intermediate layer could be chemically active, we

return to our earlier posed question of the role of coupling two Turing systems *non-linearly*. Therefore, it would be interesting to study non-linear coupling in the framework used in the above mentioned works on linearly coupled Turing systems. Here we concentrate on investigating the Brusselator model as our basic reaction-diffusion system and examine the consequences of non-linear coupling, mainly cubic coupling. We carry out extensive numerical calculations guided by linear analysis, to search for new complex patterns. A non-linear coupling means that the coupling layer is not inert like in the case of linear coupling, but there is in a sense a chemically active intermediate layer. To our knowledge, no other study has been addressing this question.

The study of coupled systems can be expanded even further. In the end of this chapter we will briefly discuss other coupling schemes, e.g. quadratic coupling. Since earlier only systems having two Turing modes have been studied, we will here introduce a system where one layer is in Turing mode but the other layer exhibits solitary wave solutions. This essentially means that we have solitons in non-integrable systems and there has been very little research in this particular field.

This chapter is organized as follows: First we will briefly go through the study made by Epstein et al. [21] and we will reproduce the patterns in order to compare those with the ones obtained with non-linear coupling. In the second part, we will introduce non-linear coupling and the last part introduces a fascinating case of having solitary waves in coupled systems.

5.1 Two-layer Brusselator model

In this section we shall investigate the possibility for obtaining complex Turing patterns from a simple set of coupled reaction-diffusion equations. The interest in this sort of research is evident when one observes real patterns in nature, which are not just the usual stripes and spots commonly found in Turing stationary patterns. As already mentioned, complicated resonant patterns have been obtained by linearly coupling two simple Turing models, each of which meet the respective Turing conditions. Here the key point is that there should be a resonance between the independent length scales of both patterns. The study by Yang et al. [21], carries out this idea by linearly coupling two systems in such a way that their respective Turing spaces are well separated, but have resonant length scales. This kind of situation can be experimentally accomplished by constructing two thin layers of gel meeting at an inert interface that allows transport of morphogens between layers. The model can be exemplified here by taking two independent Brusselators and adding a term that couples them in such a way that the amount of both pairs of morphogens is conserved.

5.1.1 Model

As for the model one could write

$$\begin{cases} \frac{\partial u_i}{\partial t} = D_{u_i} \nabla^2 u_i + \alpha(u_j - u_i) + f(u_i, v_i) \\ \frac{\partial v_i}{\partial t} = D_{v_i} \nabla^2 v_i + \beta(v_j - v_i) + g(u_i, v_i) \end{cases}, \quad (5.1)$$

where the reactive species (u and v) and their diffusion coefficients (D_u and D_v) are distinguished by subscripts $i, j = 1, 2$ ($i \neq j$) that specify the layer they are in, and both layers obey Eq.(2.11), but with different parameters. The normal two-dimensional diffusion in the layer planes is described by the Laplacian terms, and the linear coupling terms (parameters α and β) could be thought of as describing inter-layer diffusion of chemicals. As usual, the functions f and g specify the kinetic behaviour of the system. This way of coupling the systems has the virtue that a steady state solution is the same as for the 'one-layer'-model, given by Eq.(2.13). One should also notice that this way of coupling the systems produces patterns that are oscillatory in time, though fixed in space. This is evident from Eq.(5.1) if one takes the diffusion and reaction terms out, because then one ends up with a set of two coupled harmonic oscillators.

The kinetics of the system can be virtually anything, but we will now show results for the Brusselator model (ref. section 2.2). In this case the kinetics are as follows

$$\begin{cases} f(x, y) = a - (b + 1)u + u^2v \\ g(x, y) = bu - u^2v \end{cases}. \quad (5.2)$$

The calculation of steady states for one-layer-model have been done previously in section 2.2. By similar manner, one can obtain the steady-states for the model above. There will be four solutions, with one of them being the same as (2.13):

$$\mathbf{w}^0 = \begin{cases} u_1^0 = u_2^0 = a \\ v_1^0 = v_2^0 = \frac{b}{a} \end{cases}. \quad (5.3)$$

In section 2.2 we performed a linear stability analysis for the one layer Brusselator model. By using very similar techniques it can be done also in the

two-layer case although the equations will now be more complicated. In this case, the analytical solution will not (easily) give us the information we want, so we will resort to numerical solutions. Next we will briefly explain how the dispersion curves were obtained.

Now that we have two layers it means that we will have four equations and furthermore a four-by-four matrix whose eigenvalues are the ones that we are interested in. The eigenvalues can be calculated from the equation

$$|\mathbf{A} - \mathbf{D}k_j^2 - \lambda_i \mathbf{I}| = 0, \quad (5.4)$$

where matrix \mathbf{A} will be of the form

$$\mathbf{A} = \begin{pmatrix} \partial_{u_1} \hat{f}_1 & \partial_{v_1} \hat{f}_1 & \partial_{u_2} \hat{f}_1 & \partial_{v_2} \hat{f}_1 \\ \partial_{u_1} \hat{g}_1 & \partial_{v_1} \hat{g}_1 & \partial_{u_2} \hat{g}_1 & \partial_{v_2} \hat{g}_1 \\ \partial_{u_1} \hat{f}_2 & \partial_{v_1} \hat{f}_2 & \partial_{u_2} \hat{f}_2 & \partial_{v_2} \hat{f}_2 \\ \partial_{u_1} \hat{g}_2 & \partial_{v_1} \hat{g}_2 & \partial_{u_2} \hat{g}_2 & \partial_{v_2} \hat{g}_2 \end{pmatrix}.$$

Here the subscripts refer to the layers and the hat on the top of the functions f and g means that they are a sum of the Brusselator kinetics and the linear coupling term. For example we have

$$\begin{cases} \hat{f}_1 = \alpha(u_2 - u_1) + f(u_1, v_1) = \alpha(u_2 - u_1) + a - (1 + b)u_1 + u_1^2 v_1 \\ \hat{g}_1 = \beta(v_2 - v_1) + g(u_1, v_1) = \beta(v_2 - v_1) + bu_1 - u_1^2 v_1 \end{cases} \quad (5.5)$$

and similarly for \hat{f}_2 and \hat{g}_2 . All the derivatives will be evaluated at the steady-state (5.3). The matrix \mathbf{A} will then be as follows:

$$\mathbf{A} = \begin{pmatrix} -\alpha - 1 + b & a^2 & \alpha & 0 \\ -b & -\beta - a^2 & 0 & \beta \\ \alpha & 0 & -\alpha - 1 + b & a^2 \\ 0 & \beta & -b & -\beta - a^2 \end{pmatrix}.$$

The eigenvalues are calculated numerically for each value of wave number k within an appropriate interval with sufficiently small step size. At each point, the maximum value of the real part and corresponding imaginary part was plotted. Although in this case there will be four eigenvalues (because the characteristic polynomial is of fourth order) the largest one is the one that matters in most cases. Figure 5.1 shows an typical dispersion curve for the model (5.1).

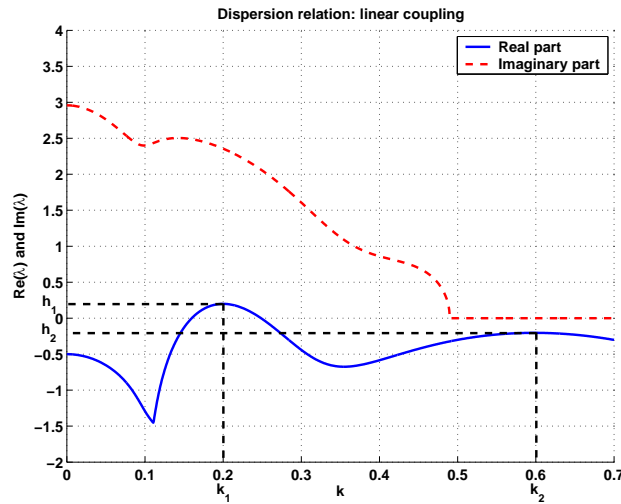


Figure 5.1: Typical dispersion curve for the linearly coupled two-layer model. Both imaginary and real part of the dominant eigenvalue have been drawn. Parameters were $a = 3$, $b = 9$, $\alpha = \beta = 1$, $D_{u_1} = 5$, $D_{v_1} = 14$, $D_{u_2} = 54.9$ and $D_{v_2} = 159.8$

5.1.2 Simulation results

In the simulations, we used as initial conditions a small random perturbation of the steady state above on each grid point. The lattice size was chosen to be 200×200 and periodic boundary conditions were applied. The parameters of simulations are given in the caption of each figure. Here the coupling parameters are equal $\alpha = \beta$ for simplicity. Next we will show some of the simulation results of the model. The images are snapshots of the system after it has reached a stable state (stationary or oscillatory). Analysis revealed that the time step has to be small enough, otherwise the simple Euler's method will not converge. Therefore we used as the time step $dt = 0.001$.

In Fig. 5.2 we present the results for the system of weak coupling, i.e. when the parameters α and β are sufficiently small ($\alpha = \beta = 0.1$). The first figure (Fig. 5.2(a)) is the so-called black-eye pattern and the second one (Fig. 5.2(b)) is the so-called white-eye pattern (although they look quite similar). The last four figures are examples of superposition patterns, each having two characteristic wavelengths. First figure (Fig. 5.3(a)) consists of black dots on long stripes, the second one (Fig. 5.3(b)) consists of small white dots on stripes, the third one is a superposition of spots of two different wave lengths and the fourth one (Fig. 5.3(d)) consists (mainly) of short thin stripes on an hexagonal array of spots.

In the black-eye patterns in Fig. 5.2 the black indicates low morphogen

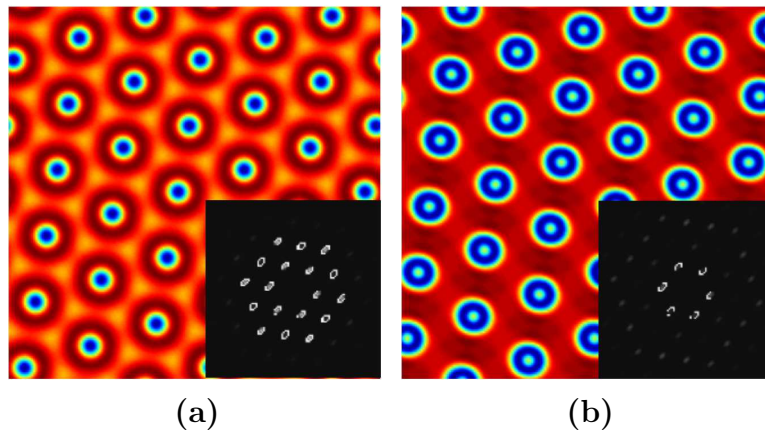


Figure 5.2: (a) Black-eye pattern with ratio near 2 : 1 obtained with the following parameters: $a = 3$, $b = 9$, $\alpha = \beta = 0.1$, $D_{u_1} = 16.7$, $D_{v_1} = 36.4$, $D_{u_2} = 49.5$ and $D_{v_2} = 117.6$. (b) White-eye pattern with ratio near 3 : 1 obtained with the following parameters: $a = 3$, $b = 9$, $\alpha = \beta = 0.1$, $D_{u_1} = 5.6$, $D_{v_1} = 12.3$, $D_{u_2} = 49.3$ and $D_{v_2} = 117.5$

concentration and the surrounding white disc indicates high morphogen concentration. In so-called white-eye patterns the situation is obviously vice versa. These eye-like spots are arranged in a hexagonal lattice and they can be understood as a resonance between two hexagonal lattices. Although these patterns look quite similar, their wave shapes are quite different. It has been observed that patterns found near a 3 : 1 wavelength ratio show white-eye and patterns near 2 : 1 and $\sqrt{3} : 1$ wavelength ratio show black-eye patterns. Similar resonant (black-eye, white-eye and superposition) patterns are found e.g. in experiments on optical systems [18]. These patterns presented here are generic in that they arise from the interaction of unstable spatial modes with appropriate ratios of wave numbers.

We also have calculated two-dimensional spatial Fourier spectrum, or amplitude spectrum, presented in the inset, for each pattern. Although those images obtained are intended to be used for qualitative analysis only, they still give valuable information of the major modes, for varying wave vectors. Such a picture in k space is also useful to detect at a glance the symmetries of the pattern. The Fourier spectrum is very often calculated for periodic, time-dependent signals. We can apply the same kind of techniques here because the patterns we are investigating are periodic, although at the moment we are not interested in the time dependent behaviour (the reader is referred to section 3.2 for further analysis). Figure 5.2(a) displays a resonance around $\sqrt{3} : 1$. The six dots in the inner circle in the Fourier spectrum of Fig. 5.2(a) indicate that there exist a hexagonal structure in the patterns (i.e. the spots).

Same kind of an interpretation can be done for the second patterns 5.2(b).

Now we show some examples of simulations producing superposition of patterns, with two characteristic wavelengths, first with weak coupling ($\alpha = \beta = 0.1$) and then with strong coupling ($\alpha = \beta = 1$). These patterns appear different from the previous ones: Each of them has two characteristic and well separated wavelengths. That conclusion can be made due to the fact that the major peaks in the two-dimensional Fourier-spectrum fall on two distinct circles in k -space. The longer wavelength patterns appear stripe-like (Figs. 5.3(a) and 5.3(b)) or, arranged as hexagonal spots (Fig. 5.3(d)). Remember that the wave number is $k = \frac{2\pi}{\lambda}$.

In the weak coupling case in Fig. 5.3(a) we see large black-eye dots forming long strings. In this case the corresponding Fourier transform (in the inset) shows very clearly the symmetry, four spots at a long wavelength revealing two preferred orientations for the strings, and a hexagonal array at a shorter wavelength corresponding to the black eye spots. In the strong coupling case in Fig. 5.3(b) we see small white-eye dots superimposed in stripes. Here the Fourier spectrum (in the inset) indicates the two-fold symmetry of the oriented stripes. Similar resonant black-eye, white-eye and superposition patterns have been found for instance in experiments on optical systems [18]. Here the patterns are generic in that they arise from the interaction of unstable spatial modes with appropriate wave number ratios.

In the third strong coupling case in Fig. 5.3(c) we see a superposition pattern of two hexagonal lattices of spots with different sizes. This is also indicated in the Fourier spectrum (in the inset) where there is some indication of long wavelength order together with a hint of short wavelength order. In the third strong coupling case depicted in Fig. 5.3(d), we show patterns which consists of short thin stripes inside spots that are arranged hexagonally. Also the Fourier spectrum, in the inset, shows very clearly the long wavelength hexagonal symmetry of spots and the four fold symmetry due to the vertical and horizontal stripes.

Another example of systems that show resonant behaviour is the Lengyel-Epstein model for the CIMA reaction [44]. In this case the kinetics are written as follows

$$\begin{cases} f(u, v) = a - \frac{4uv}{1 + u^2} \\ g(u, v) = b \left[u - \frac{uv}{1 + u^2} \right] \end{cases} \quad (5.6)$$

with parameters $(a, b) = (15, 9)$, $\alpha = \beta = 0.1$ and diffusion constants $D = (6, 80, 23, 380)$. Simulations yielded the same type of resonant patterns as

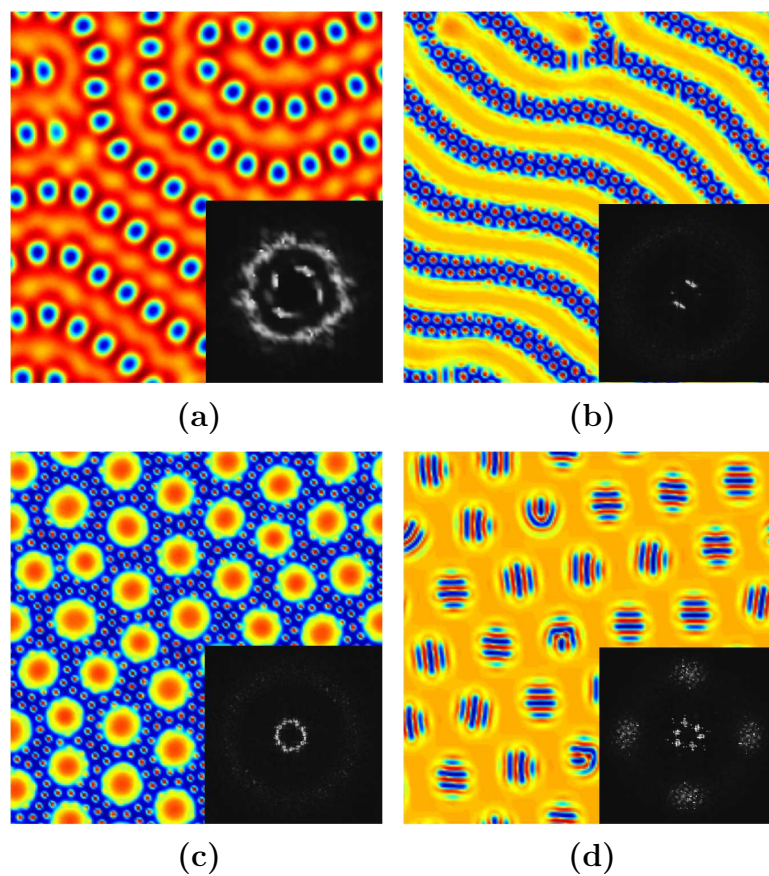


Figure 5.3: Superposition patterns obtained with the following parameters: (a) $a = 3$, $b = 9$, $\alpha = \beta = 0.1$, $D_{u_1} = 12.6$, $D_{v_1} = 27.5$, $D_{u_2} = 47.5$ and $D_{v_2} = 141.5$. (b) $a = 3$, $b = 9$, $\alpha = \beta = 1$, $D_{u_1} = 1.85$, $D_{v_1} = 5.66$, $D_{u_2} = 50.6$ and $D_{v_2} = 186.0$. (c) $a = 3$, $b = 6$, $\alpha = \beta = 1$, $D_{u_1} = 1.31$, $D_{v_1} = 9.87$, $D_{u_2} = 34.0$ and $D_{v_2} = 344.9$. (d) $a = 3$, $b = 10$, $\alpha = \beta = 1$, $D_{u_1} = 2.03$, $D_{v_1} = 4.38$, $D_{u_2} = 56.2$ and $D_{v_2} = 135.3$.

described above.

5.2 Extended Oregonator model

In previous section we analyzed a two layer model with an abstract Brusselator kinetics involving cubic autocatalysis. Here we consider a more realistic model proposed by Epstein et al. [22]. It is an extended Oregonator with quadratic autocatalysis. It mimics the BZ (Belousov-Zhabotinsky) [45] reaction. The experimental arrangement of the model presented here consists of three layers (look at the Fig. 5.4): The two layers at the top and the bottom are reaction layers and the one in the middle provides the coupling.

5.2.1 Model

The equations of this five-component reaction-diffusion model can be written as:

$$\frac{\partial x}{\partial t} = D_x \nabla^2 x + F(x, z) - \frac{1}{\delta} [x - r], \quad (5.7)$$

$$\frac{\partial z}{\partial t} = D_z \nabla^2 z + G(x, z), \quad (5.8)$$

$$\frac{\partial r}{\partial t} = D_r \nabla^2 r + \frac{1}{\delta} [x - r] + \frac{\partial}{\bar{\delta}} [u - r], \quad (5.9)$$

$$\frac{\partial u}{\partial t} = D_u \nabla^2 u + \bar{F}(u, w) - \frac{\partial}{\bar{\delta}} [u - r], \quad (5.10)$$

$$\frac{\partial w}{\partial t} = D_w \nabla^2 w + G(u, w), \quad (5.11)$$

where D_x , D_z , D_r , D_u and D_w are diffusion constants that represent the two-dimensional horizontal motion within the layers. Functions F and G are the reaction kinetics of the simple two variable Oregonator model. The terms with parameters δ and $\bar{\delta}$ give the time scale of the linear coupling between the top and the bottom layers.

The kinetic parameters ϵ , f , and q have been borrowed from the Oregonator model:

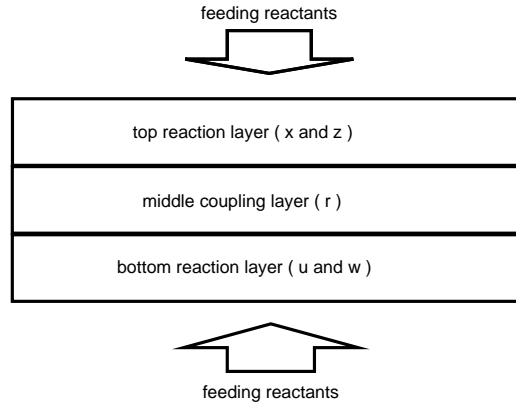


Figure 5.4: Schematic diagram of the system of coupled layers with two-sided feeding (cited from [22]).

$$\begin{cases} F(x, z) = \frac{1}{\epsilon} \left[x - x^2 - fz \frac{x - q}{x + q} \right] \\ G(x, z) = x - z \end{cases} . \quad (5.12)$$

The steady state of the basic Oregonator model can be calculated in a similar way as in the other models:

$$\begin{cases} D_x = D_z = 0 \\ \frac{\partial x}{\partial t} = \frac{\partial z}{\partial t} = 0 \end{cases} \quad (5.13)$$

This yields for the steady state the following relations:

$$\begin{cases} x = z = \frac{1}{2} \left[1 - (f + q) + \sqrt{(f + q - 1)^2 + 4q(1 + f)} \right] \\ u = w = \frac{1}{2} \left[1 - (\bar{f} + \bar{q}) + \sqrt{(\bar{f} + \bar{q} - 1)^2 + 4\bar{q}(1 + \bar{f})} \right] \end{cases} \quad (5.14)$$

We will use this as an initial condition for the simulations with a small random perturbation.

5.2.2 Simulation results

In this section we will show the results of series of simulations done with the extended Oregonator model. Due to the complexity of the patterns a very small step ($dt = 0.001$) and long simulations (10^6 steps or more) were required to obtain a stable (stationary or oscillatory) state. The size of the lattice was 256×256 and following assumptions were made for simplicity: $q = \bar{q} = 0.01$ and $\delta = 2\epsilon, \bar{\delta} = 2\bar{\epsilon}$. The Fourier spectrum has been calculated, as usual, although it gives in this case very little information as can be found in the inset of each pattern.

The patterns in Figs. 5.5(a) and (b) show a phenomenon where for a long Turing wavelengths, short wavelength traveling waves appear on the Turing structures. In these figures the Turing wavelength is about four times longer than that of the traveling waves. In Fig. 5.5(a) isolated stable spirals or sustained concentric waves (which rotate around their symmetry axis as time goes by) can be seen. In Fig 5.5(b) there are short wavelength spiral waves rotating around the oscillatory core to form “pinwheels”. First the honeycomb Turing spots arise, arrange themselves towards a hexagonal lattice, then begin to oscillate, and finally develop spirals centered on their cores. From the Fourier spectrum of both cases shown as insets the interpretation is not as clear as it was in previous simulations. This can be understood by observing from the real space patterns that although for the short range the spots seem to arrange hexagonally, for the long range the patterns are quite disordered or have dislocations, i.e. do not maintain the hexagonal symmetry.

According to [22] the waves in each of the cases in Fig. 5.5 are due to a short-wave instability. Short-wave instability generally requires at least three species and at least two levels of diffusivity, so clearly, we cannot have the short-wave instability in the uncoupled homogenous reaction-diffusion system. In addition, in these examples, the diffusion constants are equal in the wave layer. As the Fig. 4 in [22] reveals (with the same parameters as in Fig. 5.5(b)) the dispersion relations exhibit only a Hopf instability in the uncoupled top layer, a Turing instability in the uncoupled bottom layer, and both Turing and wave instabilities in the full system. It is worth noticing that these patterns are spontaneously created by the Turing instability from the homogenous uniform state meaning that no external forcing were used.

5.3 Cubic coupling

Now we move on to the non-linear coupling case. We start with cubic coupling and later on discuss briefly other possibilities of non-linear coupling.

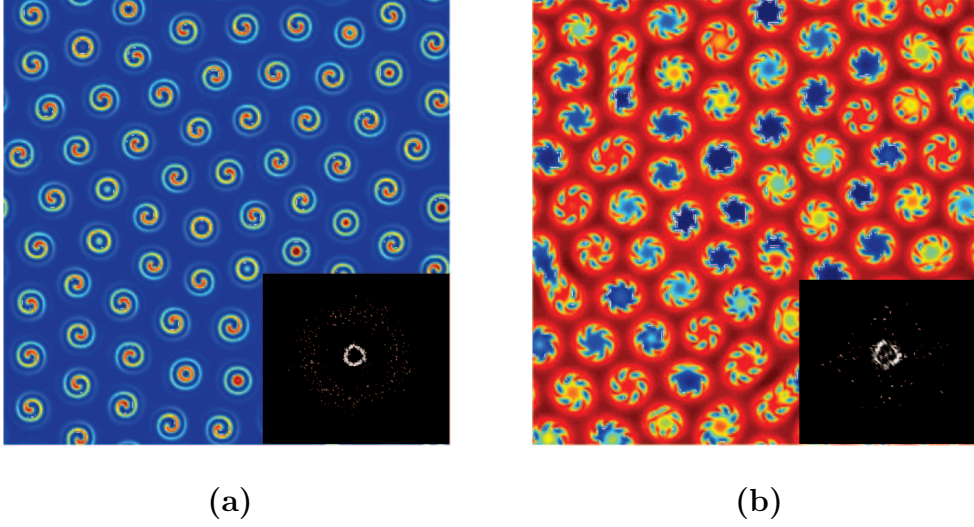


Figure 5.5: Waves on Turing structures and corresponding Fourier spectrum in the inset. Parameters are: (a) $D_x = D_z = D_r = 0.1, D_w = 100, (\epsilon, f) = (0.14, 1.6), (\bar{\epsilon}, \bar{f}) = (0.4, 1.1)$ and $D_u = 5$ (b) $D_x = D_z = D_r = 0.1, D_w = 100, (\epsilon, f) = (0.215, 1.1), (\bar{\epsilon}, \bar{f}) = (0.5, 0.65)$ and $D_u = 3$

It should be noted that a system with cubic coupling can be regarded as a model of chemical reactions between layers, contrary to the system with linear coupling which just models the flux or diffusion of the substances from one layer to the other.

5.3.1 Model

Using the model introduced in [21] as a basis, we modify it to include cubic coupling between the constituents. Moreover, we take care of morphogen conservation in the whole system, as before. Thus, our model reads as follows:

$$\begin{cases} \frac{\partial u_i}{\partial t} = D_{u_i} \nabla^2 u_i + q_1 u_i u_j (u_j - u_i) + f(u_i, v_i), \\ \frac{\partial v_i}{\partial t} = D_{v_i} \nabla^2 v_i + q_2 v_i v_j (v_j - v_i) + g(u_i, v_i), \end{cases} \quad (5.15)$$

where the notation is the same as in Eq.(5.1), except the coefficients q_1 and q_2 , which describe the strength of the coupling. Observe that now the coupling terms cannot be absorbed into a diffusion coefficient matrix, but instead they really modify the kinetics of both layers. This means that there is a kind of

intermediate layer between two real layers and it is chemically active. This model can be realized as follows: Consider a situation where we have two layers of chemicals separated by a membrane. The coupling we are using simulates the reaction of chemicals u_1 and u_2 in the intermediate layer or membrane. The same holds for the chemicals v_1 and v_2 . The concentrations of the chemicals are unbalanced on one side of the (intermediate) layer due to diffusion. Then a reaction $U_1 + 2U_2 \rightarrow P$ takes place on that side of the reactor and a reaction $P' \rightarrow 2U_1 + U_2$ on the other side respectively. P and P' are passive substances, which means that regardless of the result of the reaction, the products do not intervene in the dynamics anymore. So the result of the reaction is translated into a loss rate for the substances involved, or a feeding rate. In addition, it is not necessary that there exist any relation between the substances P and P' .

It should be noted that this realization of the coupling term is only relatively simple example. In reality the passive substances could be very complicated like energy releasing substance ATP converting into ADP as it happens in biological membranes. It is also important to notice that the substances u_1 and u_2 are different chemicals, in contrast the linear coupling where they mean the same substance in different layers.

In order to perform linear stability analysis for this model one can write the equations in the usual way around the steady state, which is still at the point given by Eq.(2.13) for both systems, namely, $u_1 = u_2 = a$ and $v_1 = v_2 = b/a$. The characteristic matrix now reads

$$\mathbf{A} = \begin{pmatrix} -a^2q_1 - 1 + b & a^2 & a^2q_1 & 0 \\ -b & -b^2q_2/a^2 - a^2 & 0 & b^2q_2/a^2 \\ a^2q_1 & 0 & -a^2q_1 - 1 + b & a^2 \\ 0 & b^2q_2/a^2 & -b & -b^2q_2/a^2 - a^2 \end{pmatrix}. \quad (5.16)$$

The dispersion relation is obtained by solving the eigenvalue problem numerically, which can then be used to search the parameter space for interesting situations and for performing numerical simulations accordingly. Obviously, the characteristic polynomial being a quartic equation gives the possibility of having two well separated Turing spaces. This implies that two very different wavelengths should be competing in a complex pattern. Here we look for values of the parameters that fulfill this requirement.

5.3.2 Simulation results

So far we have reproduced results published elsewhere (see Ref. [21, 22]), in order to compare the kind of complex patterns obtained with linearly coupled layered systems. Now, we concentrate on investigating by numerical simulations the consequences of cubic coupling in a system with periodic boundary conditions. Also for comparison, we start with the same set of parameters as used in the linear coupling case. It turns out that, in contrast to the linear case, the value of the coupling term has a great impact on the results. It was generally observed that a strong coupling usually leads to very simple patterns. Therefore, to generate any non-simple patterns the relative value of the coupling term must be small, in our simulations $q_i \approx 0.1$ or smaller. On the other hand if the cubic coupling is strong, only one wavelength will survive, and consequently only spots or stripes settle in, the occurrence of which is a general feature observed in multi-component Turing models.

Here, we are searching for superposition patterns of the kind shown in Fig. 5.3 through linear stability analysis by choosing the parameters of the system such that patterns with two well-separated wavelengths are formed. By choosing the same set of parameters as in the four patterns of the linear coupling case we obtain the patterns shown in Fig. 5.6. The main feature observed is that the system gets to the largest wavelength mode meaning that the pattern is quite simple. It is also observed that these patterns are very robust, in the sense that noise does not greatly affect their shape.

Here the only complicated pattern is in Fig. 5.6(a), which is the one corresponding to small coupling parameter. This pattern is unstable and oscillating in time, thus constantly changing but retaining the overall shape. The Fourier spectrum in the inset shows some smeared long and short wavelength behaviour. The patterns in Figs. 5.6(b)-(d) show quite simple structure of stripes, spots, and their mixture, respectively. This behaviour is attributed to strong coupling ($q_1 = q_2 = 1$). Accordingly the corresponding Fourier spectra in the insets are quite featureless with no clear structure.

We have also explored other regions of the parameter space to look for new complex patterns. To do this we have varied parameters a and b , guided by the instability regions predicted by the dispersion relations of the linear stability analysis. Once a and b were chosen, other parameters were adjusted such that there is two well separated regions of instability in the k -space. Then in the majority of simulations it turned out that if the coupling was set strong the results were the same, namely, only simple patterns were obtained. In few cases though, some interesting patterns were found.

In Fig. 5.7(a) we show a superposition pattern obtained with cubic coupling. This pattern is quite robust and similar to the one in Fig. 5.3(b), although

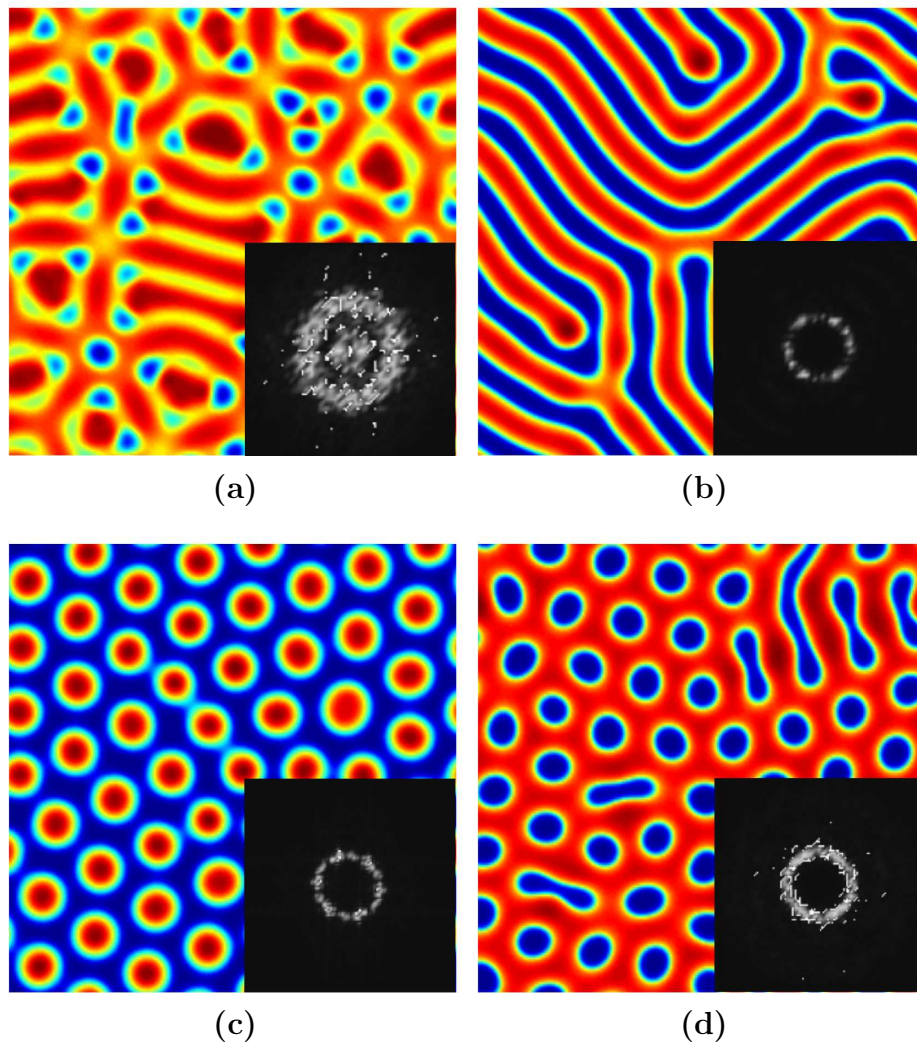


Figure 5.6: Patterns obtained using cubic coupling and the same set of parameters as in the four patterns of the linear coupling cases of Fig. 5.3, respectively. Also the cubic coupling was kept at the same values as in the linear case, that is $q_1 = q_2 = \alpha = \beta$.

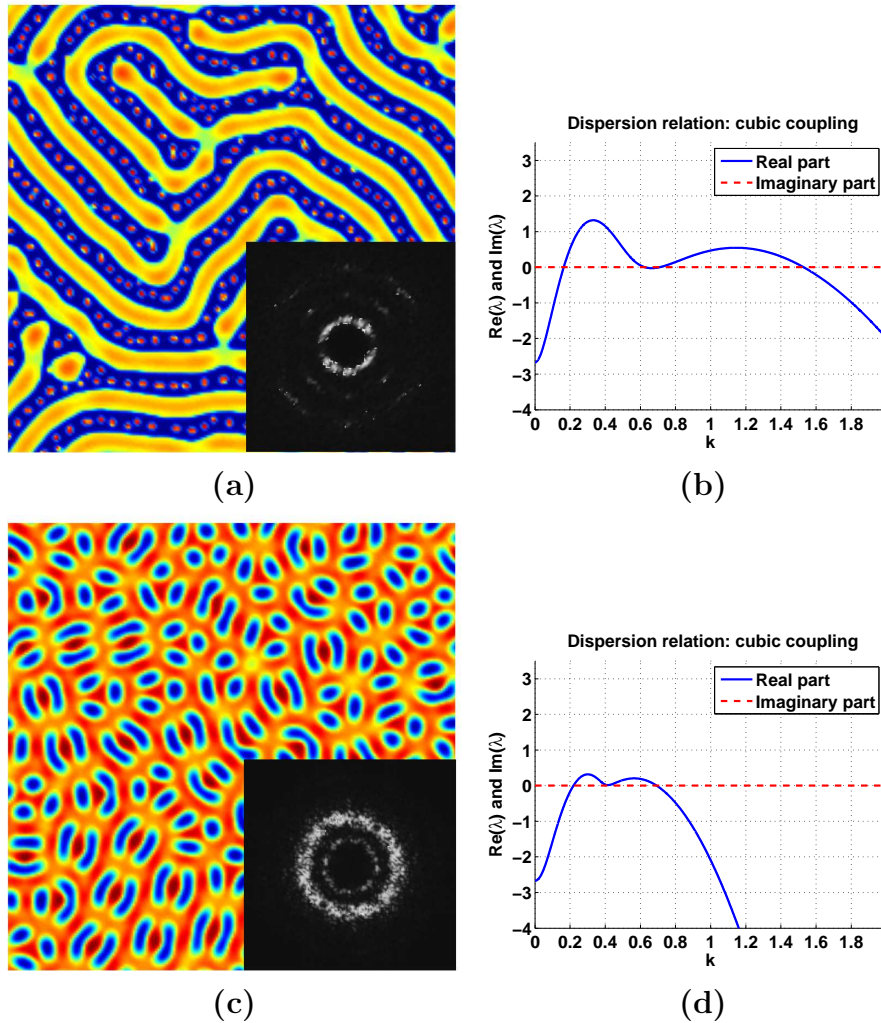


Figure 5.7: Patterns in the cubic coupling case. (a) pattern and (b) dispersion relation, respectively, for the following parameters $a = 4.5, b = 11, q_1 = q_2 = 0.1, D_{u_1} = 1.85, D_{v_1} = 16.66, D_{u_2} = 25.741$ and $D_{v_2} = 196.0$. Observe the two well separated regions of instability, resulting in a superposition of patterns. (c) pattern and (d) dispersion relation, respectively, for the following parameters: $a = 4.5, b = 11, q_1 = q_2 = 0.01, D_{u_1} = 7.5, D_{v_1} = 32.5, D_{u_2} = 27.5$ and $D_{v_2} = 121.5$. Observe that in this case the regions of instability are not well separated.

the parameters are quite different. The dispersion relation shown in Fig. 5.7(b) reveals that there are two well separated k -space regions where the modes become unstable. The resonance condition is fulfilled and a pattern with two distinct wavelengths is settled. Observe that the high k wing peaks at a value larger than one, which means that the spot pattern has a very small wavelength, so the eyes are not formed and the arrangement of spots appears more irregular than the one in Fig. 5.3(b).

Another situation is depicted in Fig. 5.7(c) where a stable pattern of bean-like shapes is seen. The dispersion relation of Fig. 5.7(d) shows that the two regions of instability in k -space are not that separated and many wavelengths can then be parametrically pumped up. The Fourier spectrum in the inset shows clearly two rings corresponding to the two regions of maximum instability in the dispersion relation. However, there is no orientational order present and there are no stripes or spots either.

The finding that complicated patterns emerge when the cubic coupling is weak, calls for more detailed analysis. To see what changes the cubic coupling brings into the pattern formation, we have made another set of simulations with varying coupling strength. For the initial starting point we choose the situation of the pattern of Fig. 5.3(b), as a good example of a linear superposition of spots and stripes with different wavelengths. By keeping all the other parameters of the system fixed, we increase the coupling strength $q_1 = q_2 = q$ in steps of $\Delta q = 0.01$ and find that this can change the emerging pattern dramatically, as depicted in Fig. 5.8 for the system of size 200×200 with periodic boundary conditions.

In the first two panels, (a) and (b), of Fig. 5.8 we show the patterns of the two layers of the system, respectively, when the layers are not coupled. These patterns are quite similar, except that the stripes have different wavelengths. In the following panels from (c) - (i) the cubic coupling is turned on and its strength is increased. In panels (c) and (d), the two coupled layers produce superimposed patterns with the two original wavelengths. We observe that appearance of the wide stripes is gradual, and that the linear superposition pattern of Fig. 5.3(b) is never reproduced. In (d) we see that the complex pattern of stripes is perturbed in some places where spots start to appear. When the coupling term was further increased the system suddenly changes to complex spot pattern of panel (e), where the spots show internal structures with a new scale. The spots themselves seem to be arranged in slightly distorted hexagonal lattice. In panel (f) we have again “spots”, but this time they have a more complicated shape resembling a boat, which indicates that the system seems to accommodate quite many wavelengths. The “boats” in panel (f) are aligned in a preferred orientation. With increasing coupling this orientation gradually dominates and produces stretching towards stripe pattern as depicted in panel (g). In panels (h) and (i) we can see that with further increase in the coupling strength the spots gradually disappear and

that a stripe like pattern with the long wavelength eventually wins. When the coupling is strong enough the pattern is again quite simple.

In Fig. 5.9(a) we can see another very good example of the effect of the coupling term. The pattern is very similar to the one in linear case (see Fig. 5.3(c) and in fact, the parameters are the same except the coupling term. The dispersion relation in Fig. 5.9(b) predicts two well separated wavelengths and we can see them in the pattern as well. When we compare this to pattern in Fig. 5.6 we can see that the long wavelength (i.e. the bigger dots) survive when the coupling is increased but the smaller dots (i.e. the short wave length) vanish. As mentioned before this seems to be a general feature in non- linearly coupled systems. One has to remember that the non-linear coupling actually affects the reaction kinetics contrary to the linear coupling where it is merely vertical diffusion. We think that the strong effect of coupling has advantages in some applications because one can dramatically change the overall pattern by simply adjusting the coupling term.

Let us now return to the very curious looking “boat” pattern, reproduced in Fig. 5.10 with the Fourier spectrum (a) and the dispersion relation (b). When the simulation run is iterated several times, the alignment of the “boats” is different and independent from the initial conditions, but the rectangular symmetry seems always to be preserved and very robust. In this study the numerical simulations were also done by using a fourth-order Runge-Kutta in order to be sure that there are no numerical artifacts. No noticeable change in the results were obtained thus giving further confidence that the numerical accuracy of the simulation method, used in this paper, is sufficient. It should be noted that there are two wings in the k -space but only one of them is clearly unstable. The high k wing moves down as the coupling increases, so for the pattern in Fig. 5.8(i) only the small k maximum is present.

5.3.3 Discussion

In this section we have concentrated on the cubically coupled model, which in the past has been dismissed on the grounds that the patterns are quite similar to the two component Turing patterns. Here the patterns found numerically are sometimes simple, as expected, but turn out to be quite complicated if the coupling strength is small. This finding is quite surprising and opposite to the linear case in which it is seen that the strength of the coupling plays practically no role in either the symmetry or the robustness of the pattern. In our study we find, however, that if the coupling is strong, only one wavelength survives and the patterns will become very simple. We consider this finding novel and potentially important.

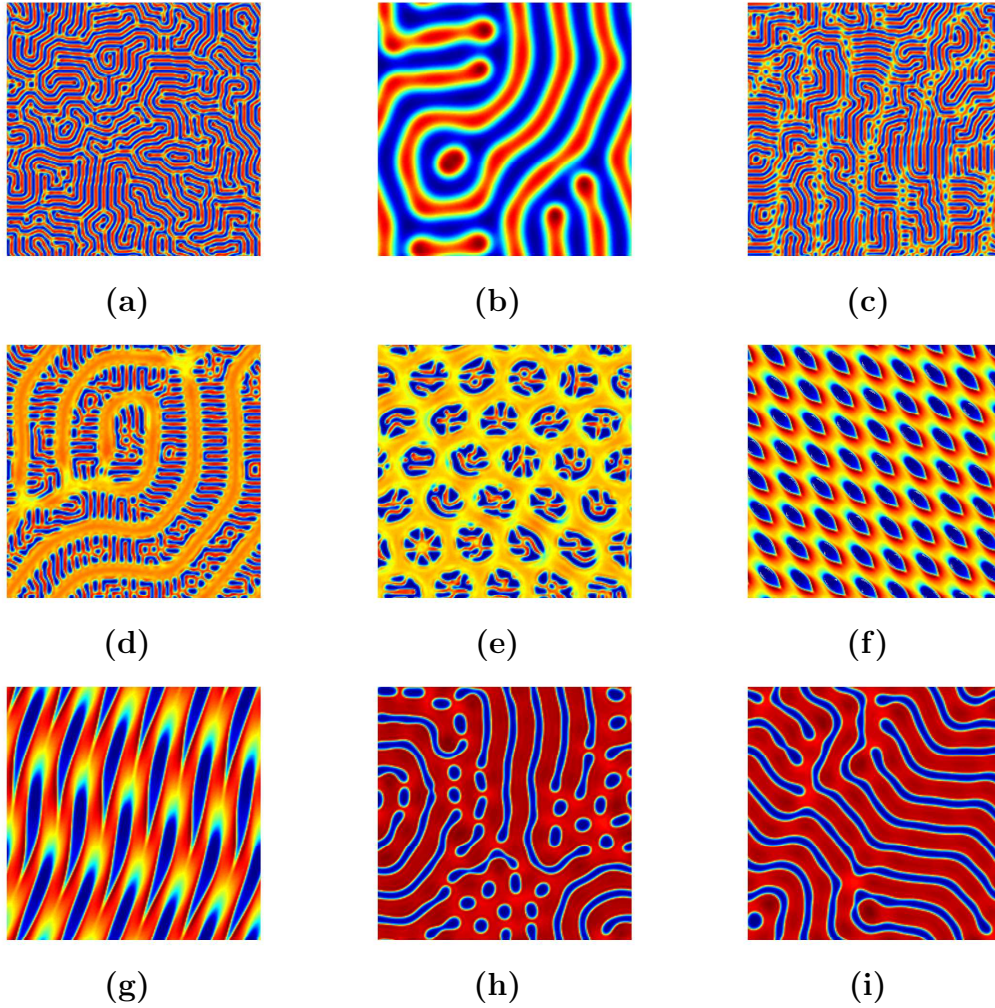


Figure 5.8: A series of patterns obtained by increasing the strength of the cubic coupling parameters $q_1 = q_2 = q$. The other parameters are the same as in Fig. 5.3 (b), namely: $a = 3$, $b = 9$, $q_1 = q_2 = 0.15$, $D_{u_1} = 1.85$, $D_{v_1} = 5.66$, $D_{u_2} = 50.6$ and $D_{v_2} = 186.0$. Panel (a) is the non-coupled pattern from layer 1 and the pattern in panel (b) is from the layer 2. In panels (c) to (i) the two layers (in panels (a) and (b)) are coupled cubically being in value 0.01, 0.05, 0.09, 0.15, 0.19, 0.27, 0.29, respectively.

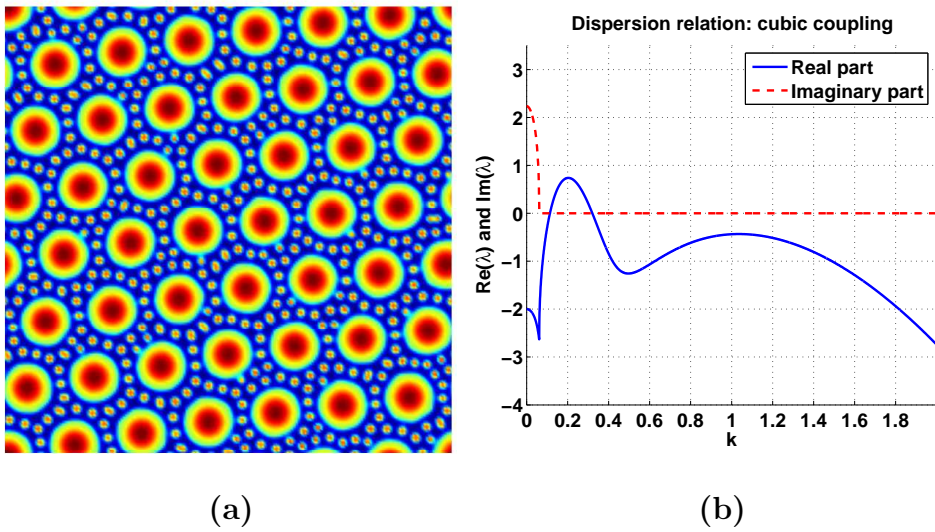


Figure 5.9: (a) A pattern of superposition of spots of two different wavelengths. Parameters are the same as in the linear case 5.3(c) but the coupling is now weaker, namely: $a = 3$, $b = 6$, $q_1 = q_2 = 0.15$, $D_{x_1} = 1.31$, $D_{y_1} = 9.87$, $D_{x_2} = 34.0$ and $D_{y_2} = 344.9$ (b) corresponding dispersion relation

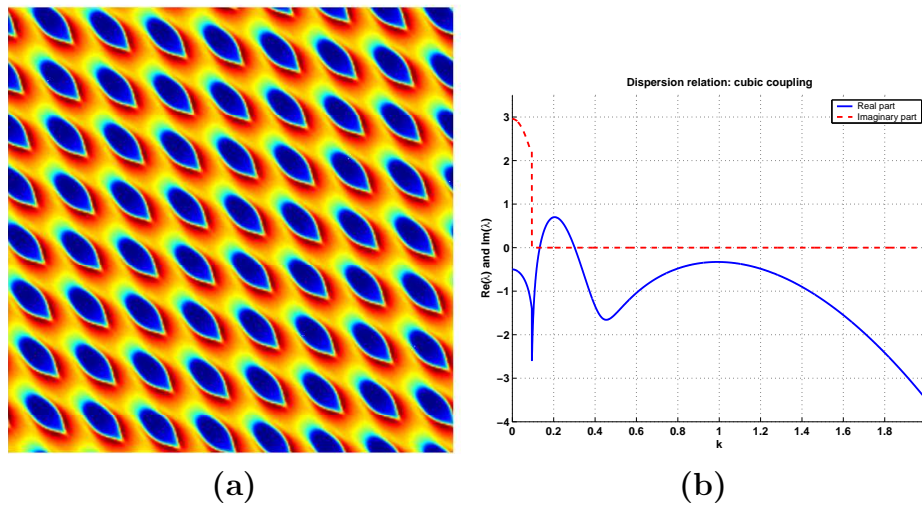


Figure 5.10: (a) The “boat”-shaped oscillatory pattern of Fig. 5.8 with the Fourier spectrum as inset and (b) the corresponding dispersion relation. Note two regions of dominant modes at $k_1 = 0.2$, $h_1 = 0.7$ and $k_2 = 1.0$, $h_2 = 0.33$.

Also, to rule out the possibility of being trapped in metastable states, in the simulations different initial conditions were tested. This is important since the system of four coupled equations is now much more complicated and the existence of other fixed points and the kind of bifurcations around them have to be explored more thoroughly. We found in general that the resulting pattern was very robustly appearing for various initial conditions. However, if one chooses a configuration near a new singular point, the system either stays there or changes completely to an unstable oscillation. This situation has to be explored in detail in the future, since it goes beyond the scope of the present study. The independence of the initial state and robustness of the pattern against strong perturbations is often a desirable feature in biological and other applications.

5.4 Other coupling schemes

In this section we will briefly introduce some new ideas we have in the framework of coupling different Turing and non-Turing systems. There are very few results available so far and therefore we limit our study here to the introduction of the models. The first one, quadratic coupling, is a direct consequence of cubic-coupling since it has the same Brusselator kinetics. The second one, the coupled BVAM-model, is novel because there the idea is to couple a Turing and a non-Turing systems with each other.

5.4.1 Quadratic coupling

In this section we will discuss quadratic coupling. Again, the (linear) analysis is very similar to the two previous models and therefore only results will be shown. The main idea here is to investigate how the coupling term affects the pattern this time. Recall that everything else, including the stable point, remains intact in these three cases. Again we are forced to resort to numerical analysis only, but hopefully some day we can investigate these phenomena more vigorously with bifurcation analysis techniques.

Let us first introduce the coupling terms (see Eq. (5.15)):

$$\begin{cases} \frac{\partial u_i}{\partial t} = D_{u_i} \nabla^2 u_i + q_1 \cdot (u_j v_i + u_i v_j) + f(u_i, v_i) \\ \frac{\partial v_i}{\partial t} = D_{v_i} \nabla^2 v_i + q_2 \cdot (u_j v_i + u_i v_j) + g(u_i, v_i) \end{cases}, \quad (5.17)$$

where u and v are the concentrations of the reactive species, D_u and D_v their diffusion coefficients respectively. The subscripts $i, j = 1, 2, i \neq j$ specify in which layer they are in. The reaction kinetics f and g are the same as in the cubic case (i.e. Brusselator, see Eq. (5.2)). As mentioned earlier, the system preserves the linear stable point

$$\mathbf{w}^0 = \begin{cases} u_1^0 = u_2^0 = a \\ v_1^0 = v_2^0 = \frac{b}{a} \end{cases}. \quad (5.18)$$

If we perform a linear stability analysis to the system above, the matrix \mathbf{A} (see (2.16) and (2.17)) will be as follows (notice that herein we have chosen $q_1 = q_2 = q$, which is not mandatory):

$$\mathbf{A} = \begin{pmatrix} q\frac{b}{a} - 1 + b & qa + a^2 & q\frac{b}{a} & qa \\ q\frac{b}{a} - b & qa - a^2 & q\frac{b}{a} & qa \\ q\frac{b}{a} & qa & q\frac{b}{a} - 1 + b & qa + a^2 \\ q\frac{b}{a} & qa & q\frac{b}{a} - b & qa - a^2 \end{pmatrix}.$$

The eigenvalues of this matrix at each value of wave number k will be calculated numerically. The characteristic polynomial will be of fourth order and at each point the maximum of the real part and corresponding imaginary part will be plotted. Figure 5.11 shows a dispersion curve. Due to the non-linear nature of the coupling, it is quite hard to predict the behaviour of the system on the basis of the dispersion relation.

Here we start the simulations similarly with the cubic case, namely, by using the same set of parameters as in the linear case. Once again, the coupling seems to have a strong effect on the pattern and very strong coupling leads to very simple patterns. The dispersion curve in Fig. 5.11 predicts that there should be two separate modes in the pattern. However, this was not the case and the patterns obtained so far are very simple, which confirms our hypothesis that only linear and cubic couplings can modify the basic stripe or spot patterns substantially. The next stage would be to first choose a very weak coupling and then gradually increase it. Then, with the help of dispersion relation, a new set of parameters can be tested in order to see, if we could have a resonance of two separate patterns.

5.4.2 Two-layer BVAM-model

In this section we will use our experience in two-layer systems into a generic reaction-diffusion system, namely the BVAM-model and show some prelim-

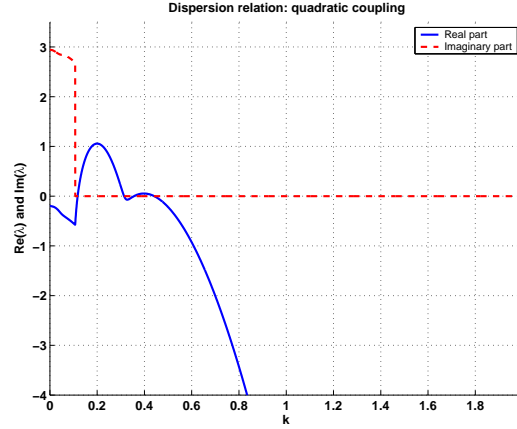


Figure 5.11: A dispersion curve for the quadratic coupled two-layer model. Both imaginary and real part of the dominant eigenvalue has been drawn. Parameters were $a = 3$, $b = 9$, $q_1 = q_2 = 0.051$, $D_{u_1} = 12.6$, $D_{v_1} = 27.5$, $D_{u_2} = 47.5$ and $D_{v_2} = 141.5$

inary results of the most recent studies. The model has been introduced earlier in 2.6 and therefore we will now omit the detailed study of this model and concentrate on the coupling. The motivation for this research comes from recent studies of BVAM-model (see [31]). It has been shown that if we extend our study outside the Turing space we can find very complicated patterns and they might have applications for instance in modelling cardiac arrhythmias [46]. Especially interesting case is the one having solitary waves in the system.

The model equations for the two-layer BVAM-model can be written as follows:

$$\begin{cases} \frac{\partial u_i}{\partial t} = D_i \nabla^2 u_i + \eta_i \alpha_i (u_j - u_i) + F(u_i, v_i) \\ \frac{\partial v_i}{\partial t} = \nabla^2 v_i + \eta_i \alpha_i (v_j - v_i) + G(u_i, v_i) \end{cases}, \quad (5.19)$$

where subscripts $i, j = 1, 2$, $i \neq j$ specify the layer of the reactive species and the kinetics are $F(u, v) = \eta(u - av - Cuv - uv^2)$ and $G(u, v) = \eta(bv + hu + Cuv + uv^2)$. The idea is the same as in (5.1), but one should notice that this time the coupling terms $\alpha_{1,2}$ are multiplied by the scaling parameter $\eta_{1,2}$ as well.

The selection of the parameters plays here an important role. First we fix the parameters for the pattern of solitary wave fronts and then find an appropriate pattern from the Turing space. In Fig. 5.12 we can see a series

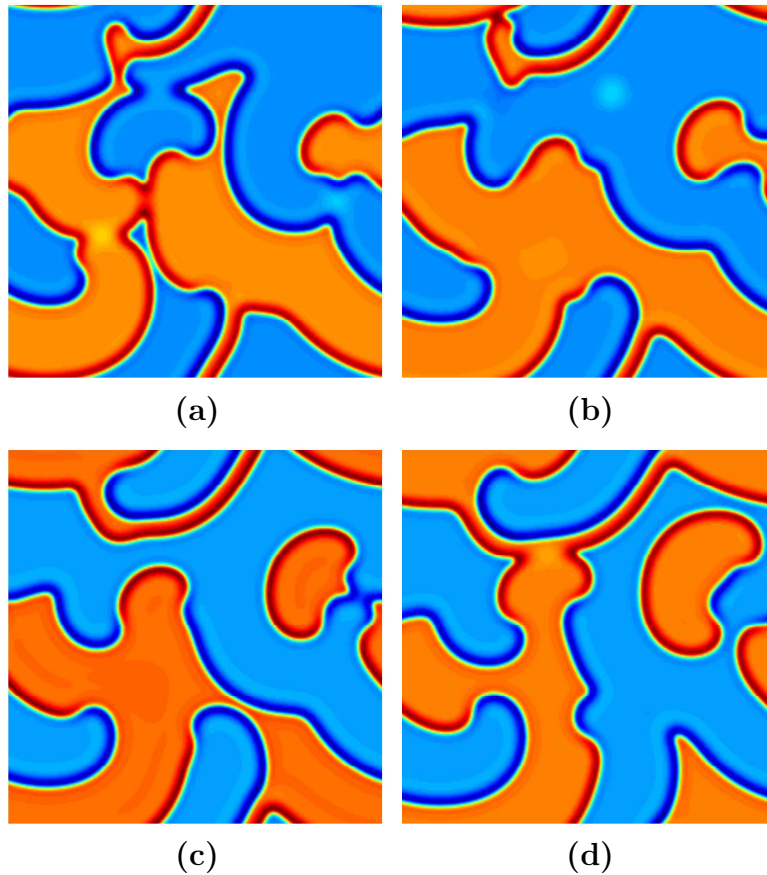


Figure 5.12: Snapshots of a pattern consisting solitary waves. The parameters are: $f = 0.65$, $g = 0.165$, $D = 1.0$, $C = 0$ and $\eta = 0.5$. The size of the lattice is 256×256 .

of snapshots of the solitary waves. The size of the lattice is 256×256 and periodic boundary conditions were applied. Throughout the simulations we use simple Euler's method and the time step here is $dt = 0.002$. The initial condition was a small random perturbation around the $\mathbf{w}_0 = (0, 0)$ fixed point. Once the system reached a stable state, we took a snapshot. Notice that in this pattern there are points that do not move but instead the fronts rotate around them. Somehow similar behaviour can be seen on the surface of cultured mono layers of cardiac myocytes (i.e. the “heartbeat”), see [47].

So far, we have managed to couple a Turing pattern and solitons both in one and two dimensions, such that the Turing pattern will attach and move with the solitons. This was done by adjusting the stable point of the Turing system to the vicinity of the peaks of the solitons.

Chapter 6

Conclusions

In this thesis, we have studied two-dimensional patterns generated by reaction-diffusion mechanism. These systems are often called Turing systems, since a British mathematician Alan Turing gave an impetus to this kind of research in 1952. His motivation was biological but here we have studied these systems from more general perspective. The novelty of this thesis lies in multi-layer systems where we introduced nonlinear coupling schemes.

In the beginning of this thesis we introduced the two-species reaction diffusion equations and a few most common reaction kinetics. We carried out a linear stability analysis in detail in order to show the reader what are the usual tools to investigate these systems. Similar analysis can be performed on multi-layer systems, as it was shown in Chapter 5, but then we usually are forced to resort numerical methods in order to find the eigenvalues of the system.

The second part of this thesis discussed briefly about the numerical methods used in the simulations. Due to the complex and nonlinear nature of the Turing systems, a numerical analysis is practically the only way to solve these equations. Special attention was paid to numerical integration methods, since incorrect use of those methods can lead to numerical artifacts and, therefore, to wrong conclusions. It was observed that if lower order methods are used, the step size has to be small enough in order to find a converged solution. Fourth-order Runge-Kutta is usually the best method for numerical integration and we used it to validate the results whenever we felt it is necessary. An adaptive step size control could make it even better, but in this particular case it was not implemented. A few ideas of Fourier analysis were presented, because we used it for analyzing the symmetries of patterns in addition to naked eye. Very much the same sort of ideas apply for pattern analysis as for signal analysis, where Fourier analysis is a common tool.

The third part of the thesis concentrated on nonlinear analysis of reaction-diffusion equations. First we discussed about dynamics and stability in general, and especially found out how we can decide if a system is stable or not. The next topic was bifurcations, which essentially describes how the dynamics of the system changes: the stabilities of the existing stationary points may change, new stable points might appear or some of the old ones might vanish. Again, simple nonlinear analysis is a very powerful tool to find the stability of these points. However, the main stress of this chapter was put into amplitude equations. We started with the complex Ginzburg-Landau equation, which describes any reaction-diffusion system close to the onset of Hopf bifurcation. Next we showed the amplitude equations for square and hexagonal Turing systems and then derived the (simplified) equations for the BVAM model. Only the derivation of the equations for the BVAM model was shown in detail since all the rest lies beyond the scope of this thesis.

The last part of the thesis concentrated on coupled systems, where most of the original work of this thesis is presented. At the beginning of the Chapter 5 we reproduced the simulations that have previously been done by Epstein's group (see [21] and [22]). This was done on the one hand, to validate our simulation programs and, on the other hand to show how the nonlinear coupling changes the patterns as all the parameters remain the same. Next, we introduced a new version, where the layers were coupled non-linearly. The main difference to earlier version is that this time the layers can actually react with each other, or to be more precise, there can be a reaction between the species in the intermediate layer. So the interface is no longer inert. We proposed that this model could simulate reactions e.g. a biological cell membrane. It has also been shown that a very similar system can model, for instance, the skin coats of some fish species (see [9]).

We noticed that in the case of nonlinear coupling the strength of the coupling plays a very important role. Therefore, in order to examine this behaviour more closely, we started with two patterns initially uncoupled and then we steadily turned on the coupling. The strength of the coupling was gradually increased, and after several iterations a snapshot was taken. It was observed that the pattern changed dramatically even though the step was very small. The last part of the Chapter 5 continued the research of coupled systems. The idea was to couple a Turing system with another pattern forming system. Essentially this was done by changing the reaction kinetics from the Brusselator model to the BVAM-model and by selecting the parameters of the other system from outside the Turing space. It turned out that we can have solitary waves in this system. This is considered to be novel because very little research has been carried out about solitons in non-integrable systems. A few, but very promising, results were obtained in coupling solitons and a Turing system but they are still under investigation.

Although only numerical analysis of the cubic-coupled system was made,

we can still draw a few conclusions: The patterns introduced are mainly quite robust and the system will not move from one pattern to another very quickly. Contrary to the linear coupling case, the strength of the coupling plays very important role in pattern formation and usually the coupling has to be very weak in order to find interesting complex patterns. If the coupling is strong, only the large wavelength survives and the patterns become very simple. Similar results have been obtained in simulations [48] and in real experiments [43]. In addition, different initial states were used to find other (meta)stable states. Different stationary states did not affect much, but if the starting point was some other pattern, it either remained almost intact or it was wiped out totally. The independence of the initial state is often desirable feature in biological and other applications. Different boundary conditions (other than periodic) were tested but the results were not encouraging and due to that we shall not include them to this thesis.

The work started here is not finished at all. Next stage would be to continue to study the problems presented in the last section of this thesis (i.e. coupling of the Turing and non-Turing systems). Another direction could be to investigate different coupling schemes with the Brusselator model. The effect of noise and different boundary conditions is also yet to be explored. The numerical analysis is a suitable tool for that, and it can be done before we get the non-linear analysis for the coupled systems.

Appendix A

Appendix

A.1 Forced complex Ginzburg-Landau equation

The forced Ginzburg-Landau equation (FCGL) describes the dynamics of the complex amplitude field in stroboscopic representation determined by multiples of the driving period. The FCGL is as follows:

$$\frac{\partial A}{\partial t} = (\mu + i\nu)A - (1 + i\alpha)|A|^2A + (1 + i\beta)\nabla^2 A + \gamma A^* \quad (\text{A-1})$$

where μ represents the distance from the Hopf bifurcation, which gives the exponential growth rate of homogenous perturbations from the $A = 0$ state, $\nu = \Omega - \omega_f/2$ is the detuning, a frequency shift, α represents nonlinear frequency correction, β represents dispersion and γ is the forcing amplitude. A^* is the complex conjugate of A and it describes the effect of the weak periodic forcing. If we split A into real and complex parts, the equation (A-1) will be as follows:

$$\begin{aligned} \frac{\partial}{\partial t} \begin{bmatrix} U \\ V \end{bmatrix} = & \left(\begin{bmatrix} \mu + \gamma & -\nu \\ \nu & \mu - \gamma \end{bmatrix} - (U^2 + V^2) \begin{bmatrix} 1 & -\alpha \\ \alpha & 1 \end{bmatrix} \right) \begin{bmatrix} U \\ V \end{bmatrix} \\ & + \begin{bmatrix} 1 & -\beta \\ \beta & 1 \end{bmatrix} \nabla^2 \begin{bmatrix} U \\ V \end{bmatrix} \end{aligned} \quad (\text{A-2})$$

Let us define a vector F :

$$\begin{aligned}
F &= \begin{bmatrix} f(U, V) \\ g(U, V) \end{bmatrix} \\
&= \begin{bmatrix} (\mu + \gamma - (U^2 + V^2))U + (-\nu + \alpha(U^2 + V^2))V \\ (\nu - \alpha(U^2 + V^2))U + (\mu - \gamma - (U^2 + V^2))V \end{bmatrix}
\end{aligned} \tag{A-3}$$

The reaction-diffusion equation has the form:

$$\frac{\partial X}{\partial t} = F(X) + \mathbf{D}\nabla^2 X \tag{A-4}$$

and the linearized version of this will be

$$\frac{\partial Y}{\partial t} = \mathbf{A}(t)Y + \mathbf{D}\nabla^2 Y \tag{A-5}$$

where $\mathbf{A}(t)$ is the Jacobian matrix:

$$\begin{aligned}
\mathbf{A}(t) &\equiv \begin{bmatrix} \frac{\partial f}{\partial U} & \frac{\partial f}{\partial V} \\ \frac{\partial g}{\partial U} & \frac{\partial g}{\partial V} \end{bmatrix} \\
&= \begin{bmatrix} -3U^2 - V^2 + 2\alpha UV + \mu + \gamma & \alpha U^2 - 2UV + 3\alpha V^2 - \nu \\ -3\alpha U^2 - 2UV + \nu - \alpha V^2 & -2\alpha UV - 3V^2 + \mu - \gamma - U^2 \end{bmatrix} \\
&= \begin{bmatrix} \mu + \gamma & -\nu \\ \nu & \mu - \gamma \end{bmatrix} + \begin{bmatrix} -3U^2 - V^2 + 2\alpha UV & \alpha U^2 - 2UV + 3\alpha V^2 \\ -3\alpha U^2 - 2UV - \alpha V^2 & -2\alpha UV - 3V^2 - U^2 \end{bmatrix}
\end{aligned} \tag{A-6}$$

When $\alpha = 0$, the equation simplifies to

$$\mathbf{M}(t) = \mathbf{L} + \mathbf{N} + \mathbf{D}, \tag{A-7}$$

where

$$\mathbf{L} = \begin{bmatrix} \mu + \gamma & -\nu \\ \nu & \mu - \gamma \end{bmatrix}, \tag{A-8}$$

$$\mathbf{N} = \begin{bmatrix} -3U^2 - V^2 & -2UV \\ -2UV & -U - 3V^2 \end{bmatrix}, \tag{A-9}$$

and

$$\mathbf{D} = \begin{bmatrix} 1 & -\beta \\ \beta & 1 \end{bmatrix} \nabla^2. \quad (\text{A-10})$$

At the fixed point $(U, V) = (0, 0)$ and with a spatial perturbation $\delta(x) = e^{\lambda t + ikx}$ the eigenvalue problem reads:

$$\begin{vmatrix} a_{11} - \lambda & a_{12} \\ a_{21} & a_{22} - \lambda \end{vmatrix} = 0 \quad (\text{A-11})$$

which implies:

$$\lambda^2 - (a_{11} + a_{22})\lambda - (a_{11}a_{22} - a_{12}a_{21}) = 0 \quad (\text{A-12})$$

$$\lambda^2 - T\lambda - \Delta = 0 \quad (\text{A-13})$$

Now $T = 2(\mu + k^2)$, and $\Delta = (\mu + k^2)^2 - \gamma^2 + (\nu - \beta k^2)$ and therefore the dispersion relation reads

$$\lambda_{1,2}(k) = \mu - k^2 \pm \sqrt{\gamma^2 - (\nu - \beta k^2)^2} \quad (\text{A-14})$$

The Hopf bifurcation takes place at

$$\mu = 0, \quad \gamma < \nu \quad (\text{A-15})$$

The onset of Turing instability requires

$$\gamma \geq \frac{-\mu\beta + \nu}{\sqrt{1 + \beta^2}}, \quad (\text{A-16})$$

and the critical Turing wavelength is

$$k_c^2 = \frac{\mu + \nu\beta}{1 + \beta^2}. \quad (\text{A-17})$$

This can be obtained by the $\lambda_1 = 0$ in Eq.(A-14) which gives

$$k^2 = \frac{\mu + \nu\beta \pm \sqrt{\psi}}{1 + \beta^2} \quad (\text{A-18})$$

where $\psi = 2\mu\nu\beta + \beta^2(\gamma^2 - \mu^2) + \gamma^2 - \nu^2$. The critical condition requires that $\psi = 0$ which gives the condition (A-16). The co-dimension Turing-Hopf conditions are then:

$$\mu_c = 0, \gamma_c = \frac{\nu}{\sqrt{1 + \beta^2}}. \quad (\text{A-19})$$

Bibliography

- [1] A.M. Turing. The chemical basis of morphogenesis. *Philos. Trans. R. Soc. London*, (B 237), 1952.
- [2] A. Gierer and H. Meinhardt. A theory of biological pattern formation. *Biological Cybernetics*, pages 30–39, 1972.
- [3] V. Castets, E. Dulos, J. Boissonade, and P. De Kepper. Experimental evidence of a sustained standing turing-type nonequilibrium chemical pattern. *Physical Review Letters*, 64(24):2953–2956, 1990.
- [4] J.D. Murray. *Mathematical Biology*. Springer-Verlag, 2003.
- [5] A. Gierer and H. Meinhardt. A theory of biological pattern formation. *Kybernetik*, 12:30–39, 1972.
- [6] S. Kondo and R. Asai. A reaction-diffusion wave on the skin of the marine angelfish *pomacanthus*. *Nature*, 376(678), 1995.
- [7] C. Varea and J.L. Aragón R.A. Barrio. Confined turing patterns in growing systems. *Physical Review E*, 56:1250, 1997.
- [8] K.J Painter, P.K. Maini, and H.G. Othmer. Stripe formation in juvenile *pomacanthus* explained by a generalized turing mechanism with chemotaxis. *Proc. Nat. Acad. Sci.*, 96:5549, 1999.
- [9] R.A. Barrio, C. Varea, J.L. Aragón, and P.K. Maini. A two-dimensional numerical study of spatial pattern formation in interacting turing systems. *Bulletin of Mathematical Biology*, 61:483–505, 1999.
- [10] R.A. Barrio and C. Varea. Non-linear systems. *Physica A*, 2006.
- [11] L.A. Segel and J.L. Jackson. *J. Theor. Biol.*, 37(545), 1972.
- [12] Y.I. Balkarei, A.V. Grigor'Yants, Y.A. Rzhanov, and M.I. Elinson. *Opt. Commun.*, 66(16), 1988.

-
- [13] S. Bose, P. Rodin, and E. Schöll. Competing spatial and temporal instabilities in a globally coupled bistable semiconductor system near codimension-two bifurcation. *Physical Review E*, 62(2), 2000.
- [14] *Self-Organization, Auto-Waves and Structures Far From Equilibrium*. Springer, Berlin, 1984.
- [15] D. Walgraef and N.M. Ghoniem. *Physical Review B*, 13(8867), 1990.
- [16] D.B. White. *J. Fluid Mech.*, 191(247), 1988.
- [17] T. Nozakura and S. Ikeuchi. *Astrophys. J.*, 279(40), 1984.
- [18] M.A. Vorontsov and B.A. Samson. Nonlinear dynamics in an optical system with controlled two-dimensional feedback: Black-eye patterns and related phenomena. *Physical Review A*, 57(4):3040–3049, Apr 1998.
- [19] M. Maruyama. *Am. Sci.*, 51(164), 1963.
- [20] P.K. Maini, K.J. Painter, and H.N.P. Chau. Spatial pattern formation in chemical and biological systems. *J. Chem. Soc., Faraday Trans.*, 93(20):3601, 3610 1997.
- [21] Lingfa Yang, Milos Dolnik, Anatol M. Zhabotinsky, and Irving R. Epstein. Spatial resonances and superposition patterns in a reaction-diffusion model with interacting turing modes. *Physical Review Letters*, 88, 2002.
- [22] Lingfa Yang and Irving R. Epstein. Oscillatory turing patterns in reaction-diffusion systems with two coupled layers. *Physical Review Letters*, 90, 2003.
- [23] G. Dewel, P. Borckmans, A. De Wit, B. Rudovics, J.-J. Perraud, E. Dulos, J. Boissonade, and P. De Kepper. Pattern selection and localized structures in reaction-diffusion systems. *Physica A*, (213):181–198, 1995.
- [24] Herman Haken. *Synergetics*. Springer-Verlag, 1983.
- [25] Steven H. Strogatz. *Nonlinear Dynamics and Chaos*. Westview Press, 2000.
- [26] T.K. Callahan and E. Knobloch. Pattern formation in three-dimensional reaction-diffusion systems. *Physica D*, (132):339–362, 1999.
- [27] Lingfa Yang, Anatol M. Zhabotinsky, and Irvine R. Epstein. Stable squares and other oscillatory turing patterns in a reaction-diffusion model. *Physical Review Letters*, 92(19), 2004.

- [28] Jeff S. McGough and Kyle Riley. Pattern formation in the gray-scott model.
- [29] Attila K. Horváth, Milos Dolnik, Anatol M. Zhabotinsky, and Irving R. Epstein. Kinetics of photoresponse of the chlorine dioxide-iodine-malonic acid reaction. *J. Phys. Chem. A*, 104(24):5766–5799, 2000.
- [30] Teemu Leppänen. *Computational Studies of Pattern Formation in Turing Systems*. PhD thesis, Helsinki University of Technology, 2004.
- [31] C. Varea, D. Hernández, and R.A. Barrio. Soliton behaviour in a bistable reaction diffusion model. *Unpublished*, 2006.
- [32] R.G. Plaza, F. Sánchez-Garduño, P. Padilla, R.A. Barrio, and P.K. Maini. The effect of growth and curvature on pattern formation. *Journal of Dynamics and Differential Equations*, 16(4):1093–1121, 2004.
- [33] Lennart Råde and Bertil Westergren. *Mathematics Handbook for Science and Engineering*. Studentlitteratur, 2001.
- [34] Igor S. Aranson and Lorenz Kramer. The world of the complex ginzburg-landau equation. *Rev. Mod. Phys.*, 74:99–143, 2002.
- [35] M. Stich. *Target patterns and pacemakers in reaction-diffusion systems*. PhD thesis, Technische Universität Berlin, 2003.
- [36] J.D. Crawford. Introduction to bifurcation theory. *Rev. Mod. Phys.*, 63(991), 1991.
- [37] T.K. Callahan and E. Knobloch. Symmetry-breaking bifurcations on cubic lattices. *Nonlinearity*, 10(1179), 1997.
- [38] M. van Hecke, P. C. Hohenberg, and W. van Saarloos. Amplitude equations for pattern forming systems. *Fundamental Problems in Statistical Mechanics VIII*, 1994.
- [39] Lingfa Yang. Nonlinear chemical dynamics and pattern formation. <http://hopf.chem.brandeis.edu/yanglingfa/pattern/>.
- [40] P.C. Matthews. Pattern formation on a sphere. *Physical Review E*, 67(036206), 2003.
- [41] J.L. Aragón, C. Varea, R.A. Barrio, and P.K. Maini. Spatial patterning in modified turing systems: Application to pigmentation patterns on marine fish. *Forma*, 13(3):213–221, 1998.
- [42] L. Yang and I.R. Epstein. Symmetric, asymmetric, and antiphase turing patterns in a model system with two identical coupled layers. *Physical Review E*, 69(2):026211, 2004.

-
- [43] I. Berenstein, M. Dolnik, L. Yang, A.M. Zhabotinsky, and I.R. Epstein. Turing pattern formation in a two-layer system: Superposition and superlattice patterns. *Physical Review E*, 70, 2004.
- [44] I. Lengyel and I.R. Epstein. *Science*, 1991.
- [45] L.F. Yang, M. Dolnik, A.M. Zhabotinsky, and I.R. Epstein. Pattern formation arising from interactions between turing and wave instabilities. *Journal of Chemical Physics*, 2002.
- [46] R.A. Barrio. *Journal of Mathematical Biology*, 2007.
- [47] G. Bub, L. Glass, and A. Shrier. Optical mapping, <http://www.cnd.mcgill.ca/bios/bub/imagebase.html>.
- [48] Lingfa Yang and Irvine R. Epstein. Symmetric, asymmetric, and antiphase turing patterns in a model system with two identical coupled layers. *Physical Review*, E 69, 2004.